Assessment of Androgen Receptor Splice Variant-7 as a Biomarker of Clinical Response in Castration-Sensitive Prostate Cancer

Adam G. Sowalsky[1], Ines Figueiredo[2], Rosina T. Lis[1], Ilsa Coleman[3], Bora Gurel[2], Denisa Bogdan[2], Wei Yuan[2], Joshua W. Russo[4], John R. Bright[1], Nichelle C. Whitlock[1], Shana Y. Trostel[1], Anson T. Ku[1], Radhika A. Patel[3], Lawrence D. True[5], Jonathan Welti[2], Juan M. Jimenez-Vacas[2], Daniel Nava Rodrigues[2], Ruth Riisnaes[2], Antje Neeb[2], Cynthia T. Sprenger[5], Amanda Swain[2], Scott Wilkinson[1], Fatima Karzai[1], William L. Dahut[1], Steven P. Balk[4], Eva Corey[5], Peter S. Nelson[3,5], Michael C. Haffner[3,5], Stephen R. Plymate[5,6], Johann S. de Bono[2,7], and Adam Sharp[2,7]

ABSTRACT

Purpose: Therapies targeting the androgen receptor (AR) have improved the outcome for patients with castration-sensitive prostate cancer (CSPC). Expression of the constitutively active AR splice variant-7 (AR-V7) has shown clinical utility as a predictive biomarker of AR-targeted therapy resistance in castration-resistant prostate cancer (CRPC), but its importance in CSPC remains understudied.

Experimental Design: We assessed different approaches to quantify AR-V7 mRNA and protein in prostate cancer cell lines, patient-derived xenograft (PDX) models, publicly available cohorts, and independent institutional clinical cohorts, to identify reliable approaches for detecting AR-V7 mRNA and protein and its association with clinical outcome.

Results: In CSPC and CRPC cohorts, *AR-V7* mRNA was much less abundant when detected using reads across splice boundaries than when considering isoform-specific exonic reads. The RM7 AR-V7 antibody had increased sensitivity and specificity for AR-V7 protein detection by immunohistochemistry (IHC) in CRPC cohorts but rarely identified AR-V7 protein reactivity in CSPC cohorts, when compared with the EPR15656 AR-V7 antibody. Using multiple CRPC PDX models, we demonstrated that AR-V7 expression was exquisitely sensitive to hormonal manipulation. In CSPC institutional cohorts, AR-V7 protein quantification by either assay was associated neither with time to development of castration resistance nor with overall survival, and intense neoadjuvant androgen-deprivation therapy did not lead to significant AR-V7 mRNA or staining following treatment. Neither pre- nor posttreatment AR-V7 levels were associated with volumes of residual disease after therapy.

Conclusions: This study demonstrates that further analytical validation and clinical qualification are required before AR-V7 can be considered for clinical use in CSPC as a predictive biomarker.

Introduction

Prostate cancer is one of the most common malignancies in men and is a leading cause of male cancer-related death globally (1). The androgen receptor (AR) remains the major therapeutic target in advanced prostate cancer and AR-targeting therapies have improved the outcomes of patients with advanced castration-sensitive prostate cancer (CSPC) and castration-resistant prostate cancer (CRPC; refs. 2, 3). Despite these advances, primary and secondary resistance to therapies targeting the AR signaling axis, which include luteinizing hormone-releasing hormone analogues, abiraterone, enzalutamide, darolutamide, and apalutamide, is inevitable (3). Taken together, the development of analytically validated and clinically qualified predictive biomarkers that identify those patients who benefit from therapies targeting the AR is an area of urgent unmet clinical need; such tests optimize clinical benefit and quality of life while reducing the treatment-related and financial toxicity associated with these treatments.

Resistance to therapies targeting the AR is, in part, driven by the emergence of *AR* amplification and mutations, which invariably impact clinically available AR inhibitors that function through the AR C-terminal ligand-binding domain (LBD; refs. 4–8). In addition, constitutively active AR splice variants, of which AR splice variant-7 (AR-V7) is the most frequently observed, are considered both a

[1]Center for Cancer Research, NCI, NIH, Bethesda, Maryland. [2]Institute of Cancer Research, London, UK. [3]Fred Hutchinson Cancer Research Center, Seattle, Washington. [4]Beth Israel Deaconess Medical Center, Boston, Massachusetts. [5]University of Washington, Seattle, Washington. [6]Geriatrics Research, Education and Clinical Center, VAPSHCS, Seattle, Washington. [7]Royal Marsden NHS Foundation Trust, London, UK.

Johann S. de Bono and Adam Sharp contributed equally and share senior authorship of this article.

Corresponding Authors: Adam G. Sowalsky, NCI, 37 Convent Drive, Building 37, Room 1062B, Bethesda, MD 20892. Phone: 240-760-7118; E-mail: adam.sowalsky@nih.gov; Johann de Bono, Institute of Cancer Research, 15 Cotswold Road, Sutton, Surrey SM2 5NG, UK. Phone: 44-0-208-722-4029; E-mail: johann.de-bono@icr.ac.uk; and Adam Sharp, Institute of Cancer Research, 15 Cotswold Road, Sutton, Surrey, SM2 5NG, UK. Phone: 44-0-203-437-6562; E-mail: adam.sharp@icr.ac.uk

Clin Cancer Res 2022;28:3509–25

doi: 10.1158/1078-0432.CCR-22-0851

Translational Relevance

Although androgen receptor (AR)-targeting therapies were initially approved for metastatic castration-resistant prostate cancer (CRPC), recent clinical trials have demonstrated their efficacy in hormone-naïve and newly diagnosed castration-sensitive prostate cancer (CSPC). Expression of the AR splice variant AR-V7 is a predictive biomarker for resistance to AR-targeted therapies in CRPC, but its status in CSPC is controversial. In this study, we used a robustly validated antibody against AR-V7 in tissues from multiple CSPC clinical cohorts treated with AR-targeting therapies and found that AR-V7 status at baseline was not associated with clinical outcome. In addition, we found that using splice junction-sensitive RNA-seq most closely correlates with AR-V7 levels at the protein level across all cohorts. These findings underscore the importance of careful antibody validation and the use of rigorous controls when new IHC assays are translated to clinical practice.

potential driver of resistance and a clinically validated biomarker for patient treatment stratification in CRPC (9–14). AR-V7 typically arises from alternative mRNA splicing that leads to loss of exons 4–8, and inclusion of cryptic exon 3 (CE3), with the resultant protein product remaining transcriptionally active through its N-terminal domain, while lacking the C-terminal LBD (15, 16). AR-V7 drives the growth of prostate cancer cell lines and prostate cancer patient-derived mouse xenografts (PDX) in the presence of therapies targeting the AR (15–17). Furthermore, retrospective clinical studies have demonstrated that AR-V7 mRNA and protein from tissue biopsies and blood (circulating tumor cells and whole blood) are associated with resistance to therapies targeting the AR (9, 11–14, 18). More importantly, a prospective study demonstrated that AR-V7 mRNA- and protein-positive circulating tumor cells are associated with worse outcomes (progression-free survival and overall survival) of patients with CRPC receiving AR-targeted therapies, although it is important to acknowledge the challenges and limitations of AR-V7 biomarker development in CRPC (10, 19–24).

As AR-targeting therapies continue to demonstrate efficacy earlier in disease course, the development of predictive biomarkers remains critical (25–30). Although the role of AR-V7 as a predictive biomarker in advanced CRPC is well studied, its relevance in untreated primary prostate cancer is far less clear (31–36). The purpose of this study was to evaluate the significance of AR-V7 expression in primary CSPC. We interrogated the sensitivity and specificity of different measurement approaches to quantify AR-V7 mRNA and protein in multiple prostate cancer models including cell lines and patient-derived models, translating these approaches to multiple independent CSPC patient cohorts with associated clinical outcomes. Here, we demonstrate that AR-V7 is expressed at low mRNA and protein levels in untreated primary CSPC compared with CRPC. Using multiple cell lines, patient-derived models, and independent CSPC patient cohorts, we demonstrate in independent laboratories that AR-V7 protein expression determined by IHC using the CRPC-validated RM7 AR-V7 antibody shows strong specificity for AR-V7. We further show that baseline levels of AR-V7 detected by both IHC and AR-V7–specific splice junctions in RNA sequencing (RNA-seq) do not predict clinical outcomes in CSPC treated with AR-targeted therapies in multiple clinical settings. Our analyses confirm that in the context of current measurement approaches, AR-V7 expression in untreated, primary CSPC is extremely low with AR-V7 testing and therefore unlikely to play a major role as a predictive biomarker in this setting.

Materials and Methods

Cell lines

The following cell lines were used: 22Rv1 (ATCC; cat. #CRL-2505, RRID:CVCL_1045), VCaP (ATCC; cat. #CRL-2876, RRID:CVCL_2235), LNCaP (ATCC; cat. #CRL-1740, RRID:CVCL_1379), C42 (ATCC; cat. #CRL-3314, RRID:CVCL_4782), DU145 (ATCC; cat. #HTB-81, RRID:CVCL_0105), PC3 (ATCC; cat. #CRL-1435, RRID:CVCL_0035), and PNT2 (Sigma-Aldrich; cat. #95012613, RRID:CVCL_2164). LNCaP95 cells (RRID:CVCL_ZC87) were provided by Alan K. Meeker and Jun Luo (Johns Hopkins University, Baltimore, MD). All cell lines were grown in recommended media at 37°C in 5% CO_2. Cell lines were tested for *mycoplasma* using the VenorGem One Step PCR Kit (Cambio) and short tandem repeat profiled at regular intervals. Formalin-fixed, paraffin-embedded (FFPE) cell line pellets (containing 4 to 5 million cells) for IHC were developed by fixing overnight, at 4°C, in 10% neutral buffered formalin. The following day, fixed pellets were either processed through to paraffin block or transferred to 70% ethanol and kept, at 4°C, until being processed.

Immunoblotting

Immunoblotting methods have been previously described (14). Briefly, cells were lysed with RIPA buffer (ThermoFischer Scientific) supplemented with protease inhibitor cocktail (ThermoFischer Scientific). Protein extracts (25 μg) were separated on 4/12% NuPAGE Bis-Tris gel (Invitrogen) by electrophoresis and subsequently transferred onto Immobilon-P PVDF membranes of 0.45 μm pore size (Millipore). Primary antibodies used were: rabbit monoclonal anti–AR-V7 (1 in 1,000, RevMAb Biosciences clone RM7; cat. #31-1109-00, RRID:AB_2716436), rabbit monoclonal anti–AR-V7 (1 in 1,000, Abcam clone EPR15656; cat. #ab198394, RRID:AB_2861275), AR N-terminus (1 in 1,000, Agilent Technologies clone AR441; cat. #M356201-2, RRID:AB_2060174), AR C-terminus (1 in 1,000, Abcam clone EP670Y; cat. #ab52615, RRID:AB_867653), and GAPDH (1 in 5,000, Santa Cruz Biotechnology clone 6C5; cat. #sc-32233, RRID:AB_627679) with species-specific secondary antibodies conjugated to horseradish peroxidase. Chemiluminescence was detected using ECL substrate (Bio-Rad) on the Chemidoc Touch imaging system (Bio-Rad).

VCaP mouse xenograft models

VCaP mouse xenograft models have been previously described (14, 37). Briefly, all animal studies were performed in accordance with Beth Israel Deaconess Medical Center IACUC regulations (protocol 086-2016). VCaP cells (5 million) in 100% Matrigel were injected subcutaneously into 6-week-old 'ICR scid' mice (Taconic Biosciences). Xenografts were grown until 1,000 mm^3; then mice were castrated. For abiraterone acetate (AA)- and enzalutamide (E)-resistant xenograft models, when castrated tumors exceeded 150% nadir volume, they were treated with AA (30 mg/kg) and E (50 mg/kg). Tumors were biopsied before castration resistance (castration sensitive, CS), at castration resistance (castration resistant, CR), and when resistant to AA and E therapy (AA/E resistant, AA/E R).

Patient-derived mouse xenografts

Institute of Cancer Research (ICR) patient-derived models: All animals were housed in pathogen-free facilities. All mouse work was carried out in accordance with the ICR guidelines, including approval by the ICR Animal Welfare and Ethical Review Body, and with the UK Animals (Scientific Procedures) Act 1986. The CP50 PDX was derived from a metastatic lymph node biopsy from a patient with CRPC who had received docetaxel, abiraterone, cabzitaxel, and enzalutamide treatment for CRPC as previously described (38, 39). A second PDX, CP89, derived from a metastatic lymph node biopsy from a patient with mismatch repair–deficient CRPC who had received abiraterone for CSPC and, docetaxel and enzalutamide for CRPC, was developed. A further subline of the CP50 and CP89 PDXs was developed that was grown and maintained exclusively in castrate mice (CP50C and CP89C). Experimental conditions are described in associated figure legends.

University of Washington (UW) patient-derived models: All PDX experiments were approved by the UW Institutional Animal Care and Use Committee (protocol no. 3202-01). LuCaP PDX lines were established from specimens acquired at either radical prostatectomy or at autopsy, implanted, and maintained by serial passage in immune-compromised male mice as described previously (40).

Biospecimen procurement

ICR and Royal Marsden Hospital (RMH) patient cohorts: Patients were identified from a population of men with CRPC treated at the RMH. All patients had given written informed consent and were enrolled in institutional protocols approved by the RMH ethics review committee (reference no. 04/Q0801/60). Human biological samples were sourced ethically, and their research use was in accordance with the terms of the informed consent provided. All tissue blocks were freshly sectioned and were considered for IHC analyses only if adequate material was present. Demographic and clinical data for each patient were retrospectively collected from the hospital's electronic patient record system.

UW patient cohorts: The Institutional Review Board of the UW gave approval for this work with the UW cohort. The UW cohort consisted of 26 men who received radical prostatectomy without neoadjuvant therapy. A tissue microarray (TMA) of FFPE tissues with a total of 206 cores containing primary prostate acinar adenocarcinomas, tumor-adjacent benign prostatic tissues, and benign control tissues was generated and used in this study.

NCI patient cohorts: The collection and analysis of tissue and demographic data from patients with high-risk localized prostate cancer treated with androgen-deprivation therapy (ADT) plus enzalutamide prior to surgery were approved by the NIH Institutional Review Board (protocol 15-c-0124). The collection and analysis of tissue and demographic data from patients with localized prostate cancer treated only by surgery were approved by the institutional review boards of the Beth Israel Deaconess Medical Center (protocol 2010-P-000254/0) and the Dana-Farber/Harvard Cancer Center (protocols 15-008 and 15-492). All patients provided informed consent before participation. This research was conducted in accordance with the principles of the Declaration of Helsinki.

IHC

ICR and RMH IHC: AR-V7 (RevMAb Biosciences clone RM7 and Abcam clone EPR15656) and AR N-terminal (NTD) IHC assays have been previously described (14, 41). Briefly, RM7 IHC was performed using recombinant rabbit monoclonal anti–AR-V7 antibody (RevMAb Biosciences clone RM7; cat. #31-1109-00, RRID: AB_2716436). FFPE cell lines, PDXs, and patient tissue biopsies were first deparaffinized before antigen retrieval by microwaving (in Tris/EDTA buffer, pH 8.1) for 18 minutes at 800 W, and anti–AR-V7 antibody (1 in 500 to 1 in 50 dilution in Dako REAL diluent, Agilent Technologies) was incubated with tissue for 1 hour at room temperature. After washing, the bound antibody was visualized using the Dako Real EnVision Detection System (Agilent Technologies). Sections were counterstained with hematoxylin. Cell pellets from 22Rv1 (positive) and PC3 (negative) were used as controls. Rabbit IgGs were used as a further negative control. EPR15656 IHC assay was performed using recombinant rabbit monoclonal anti–AR-V7 antibody (Abcam clone EPR15656; cat. #ab198394, RRID:AB_2861275). Biopsies were first deparaffinized before antigen retrieval by microwaving (citrate buffer, pH6) for 18 minutes at 800 W. Blocking was performed using the protein block solution from the Novolink polymer detection system (Leica), and anti–AR-V7 antibody (1 in 200 to 1 in 50 dilution in Dako REAL diluent, Agilent Technologies) was incubated with tissue for 1 hour at room temperature. The reaction was visualized using the Novolink polymer and DAB chromogen. Sections were counterstained with hematoxylin. Cell pellets from 22Rv1 (positive) and DU145 (negative) were used as controls. Rabbit IgGs were used as a further negative control. AR-NTD IHC was performed using mouse monoclonal anti–AR-NTD antibody (Agilent Technologies clone AR441; cat. #M356201-2, RRID:AB_2060174). Biopsies were first deparaffinized before antigen retrieval using pH 8.1 Tris/EDTA solution heated in a water bath, and anti–AR antibody (1 in 1,000 dilution in Dako REAL diluent, Agilent Technologies) was incubated with tissue for 1 hour at room temperature. After washing, the bound antibody was visualized using Dako Real EnVision Detection System (Agilent Technologies). Sections were counterstained with hematoxylin. Cell pellets from VCaP (positive) and PC3 (negative) were used as controls. Mouse IgGs were used as a further negative control. AR C-terminal (CTD) IHC was performed using recombinant rabbit monoclonal anti–AR-CTD antibody (Abcam clone EP670Y; cat. #ab52615, RRID:AB_867653). Biopsies were first deparaffinized before antigen retrieval using a pressure cooker (Menapath Antigen Access Unit) in citrate buffer (pH 6), and anti–AR-CTD antibody (1 in 100 dilution in Dako REAL diluent, Agilent Technologies) was incubated with tissue for 1 hour at room temperature. After washing, the bound antibody was visualized using Dako Real EnVision Detection System (Agilent Technologies). Sections were counterstained with hematoxylin. Cell pellets from 22Rv1 (positive) and PC3 (negative) were used as controls. Rabbit IgGs were used as a further negative control.

UW IHC: Following deparaffinization, slides were steamed for 45 minutes in 1× Target Retrieval Solution (Agilent Technologies) and blocked with dual endogenous enzyme block for 10 minutes (Agilent Technologies). Tissues were then incubated with anti–AR-V7 antibody (RevMAb Biosciences clone RM7; cat. #31-1109-00, RRID: AB_2716436) at 1 in 50 at 37°C for 1 hour in antibody diluent (Ventana). Primary antibody complexes were detected using the UltraVision Quanto Detection System (Thermo Fisher) as described previously (42). Tissues were counterstained with hematoxylin, mounted, and imaged on a Ventana DP 200 Slide Scanner (Roche). FFPE LNCaP95 cell line pellets and LuCaP 77CR PDX tissues were used as positive controls.

NCI IHC: For IHC with AR [Cell Signaling Technology clone D6F11; cat. #5153, RRID:AB_10691711), diluted 1:200 into Biocare Renoir Red diluent (Biocare Medical)] or AR-V7 [RevMAb Biosciences clone RM7; cat. #31-1109-00, RRID:AB_2716436, diluted 1:100 into SignalStain Antibody Diluent (Cell Signaling)], IHC assay

was performed in FFPE human tissue sections, slides were baked for 30 minutes at 60°C, deparaffinized through xylenes, and rehydrated through graded alcohols. Antigen retrieval was performed using a NxGen Decloaker (Biocare Medical), for 15 minutes at 110 °C in Tris-EDTA Buffer, pH 9.0 (Abcam) for AR-V7 or for 15 minutes at 110°C in Diva Decloaker (Biocare Medical) for AR. Slides were loaded into an intelliPATH FLX autostainer (Biocare Medical). Blocking was performed with 3% hydrogen peroxide (Fisher Scientific) for 5 minutes and Background Punisher (Biocare Medical) for 10 minutes, then incubated with the primary antibody for 30 minutes at room temperature. Secondary labeling was performed with the Mach 4 Universal HRP Polymer Kit (Biocare Medical). Colorimetric detection was achieved using Betazoid DAB (Biocare Medical) for 3 minutes, and counterstaining was performed using CAT Hematoxylin (Biocare Medical). After dehydration through graded alcohols and clearing in xylenes, slides were mounted with Permount (Fisher Scientific). Cell pellets from VCaP CRPC xenografts were used as positive controls for AR-V7. Human tissue served as internal negative and positive controls for AR-NTD.

IHC quantification

Nuclear and cytoplasmic AR-V7 staining was determined for PDXs and patient tissue biopsies by a pathologist (author D.N.R., B.G., M.C.H., or R.T.L.) blinded to clinical data using the modified H-score method, a semiquantitative assessment of staining intensity that reflects antigen concentration. H-score was determined according to the formula: ([% of weak staining] × 1) + ([% of moderate staining] × 2) + ([% of strong staining] × 3), yielding a range from 0 to 300 (43).

RNA-seq and analysis

ICR and RMH RNA-seq: CP50 and CP89 PDX experiment RNA was extracted, and RNA-seq was performed as previously described (38). Paired-end transcriptome reads were aligned to the human reference genome (GRCh38/hg38) using the STAR (RRID: SCR_004463) splice-aware aligner (v2.7.7a) with default settings for the two-pass method. Reads aligning to the mouse reference genome (GRCm38/mm10) were discarded using the XenofilteR package (v1.6; ref. 44). For *AR-V7* splice junction analysis, reads mapping uniquely to Ex3–CE3 junction were quantified in the range chrX:67686127–67694672. Spliced reads per million were reported for each sample.

UW RNA-seq: Total RNA was isolated from flash-frozen LuCaP PDX tissues or cell lines with RNA STAT-60 (Tel-Test) followed by purification with the RNeasy Mini Kit (Qiagen) using the manufacturer's recommended in-solution DNase digestion (Qiagen). RNA concentration, purity, and integrity were assessed by NanoDrop 2000 (Thermo Fisher Scientific) and 2100 Bioanalyzer (Agilent Technologies). RNA-seq libraries were constructed from 1 μg total RNA using the Illumina TruSeq Stranded mRNA LT Sample Prep Kit according to the manufacturer's protocol. Barcoded libraries were pooled and sequenced by Illumina NovaSeq 6000 or HiSeq 2500 generating 50 bp paired-end reads. Sequencing reads were mapped to the hg38 human genome and mm10 mouse genomes using the STAR 2.7.3a two-pass method (45). Sequences aligning to the mouse genome deriving from potential contamination with mouse tissue were removed from the analysis using XenofilteR (v1.6; ref. 44).

NCI RNA-seq: FFPE tissues were lysed in 1.5 mL microcentrifuge tubes using the RNeasy FFPE Mini Kit (Qiagen) according to the manufacturer's instructions. Recovered RNA (100–600 ng) was assembled into strand-specific, paired-end, Illumina-compatible sequencing libraries using the NEBNext Ultra II Directional RNA Library Prep Kit (New England Biolabs) with the NEBNext rRNA Depletion Kit (New England Biolabs). Libraries were quantified, pooled, and sequenced paired-end on a NovaSeq S4 flowcell with 100 cycles paired-end (2 × 100). Demultiplexed FASTQ files were adaptor-trimmed using Trimmomatic (RRID:SCR_011848) version 0.36 (46) and aligned to GRCh38 using the STAR 2.7.0f two-pass method (45), with an average of 24.9 million mapped reads (range, 8.0 to 47.8 million mapped reads) per sample.

AR splice junction analysis: Splice junction analysis was performed on cohorts from ICR/RMH, UW, and NCI, as well as cases from the genotype–tissue expression (GTEx), The Cancer Genome Atlas (TCGA), and West Coast Dream Team–metastatic CRPC (WCDT–mCRPC) cohorts. GTEx data were downloaded from the NHGRI Genomic Data Science Analysis, Visualization, and Informatics Lab-Space (AnVIL; https://gen3.theanvil.io/) and TCGA and WCDT-mCRPC data were downloaded from the NCI Genomic Data Commons (https://gdc.cancer.gov/). Splice junctions from all cohorts were extracted from STAR-aligned BAM files using the sjFromSAMcollapseUandM.awk script in the STAR package. The precise number of reads in each alignment mapping to Ex3-Ex4 were defined by the chrX:67686127–67711401 junction, whereas reads mapping to Ex3-CE3 were defined by the chrX:67686127–67694672 junction. Spliced and unspliced reads mapping exclusively to CE3 were processed as described previously (47). Spliced reads or mapped reads were quantified as spliced reads per million or mapped read counts per million.

AR-V7 signature score quantification

AR-V7 signature scores were derived using the 59-gene set reported previously (14). Log_2-transformed FPKM values for all human or PDX cohorts were compiled and passed to GSVA (48) for R using the parameters method = "gsva" and kcdf = "Gaussian." The scores reported are the ES enrichment score for each sample.

Statistical analysis

Statistical analyses were performed with GraphPad Prism (RRID: SCR_002798) version 9.2.0 (GraphPad Software). Associations between factors were measured using Spearman correlations. Comparisons of single factors between treated and untreated tumors were performed using Mann–Whitney or Welch *t* tests. Null hypothesis tests of enrichments between AR-V7–positive and –negative tumors and individual dichotomous factors were performed using two-sided Fisher exact tests. Statistical significance was prespecified at $P < 0.05$. All tests used are described in figure legends.

Data availability

Raw sequencing data from human prostate tumors were deposited into the NCBI Database of Genotypes and Phenotypes at https://www.ncbi.nlm.nih.gov/gap/ and can be accessed with phs001813.v2.p1 and phs001938.v3.p1. GTEx data are available from the NHGRI Genomic Data Science AnVIL (https://gen3.theanvil.io/) and TCGA and WCDT-mCRPC data are available from the NCI Genomic Data Commons (https://gdc.cancer.gov/).

Results

AR-V7 mRNA expression is low in primary prostate cancer when spliced reads are evaluated

AR-V7 has been suggested to be a clinical biomarker in untreated primary prostate cancer; its precise enumeration is therefore paramount. We assessed methods for detecting *AR-V7* transcriptomically by inspecting spliced and unspliced read pileups using the Integrative Genome Viewer (IGV) in multiple data sets. This allowed us to distinguish intronic whole transcriptome sequencing reads that also

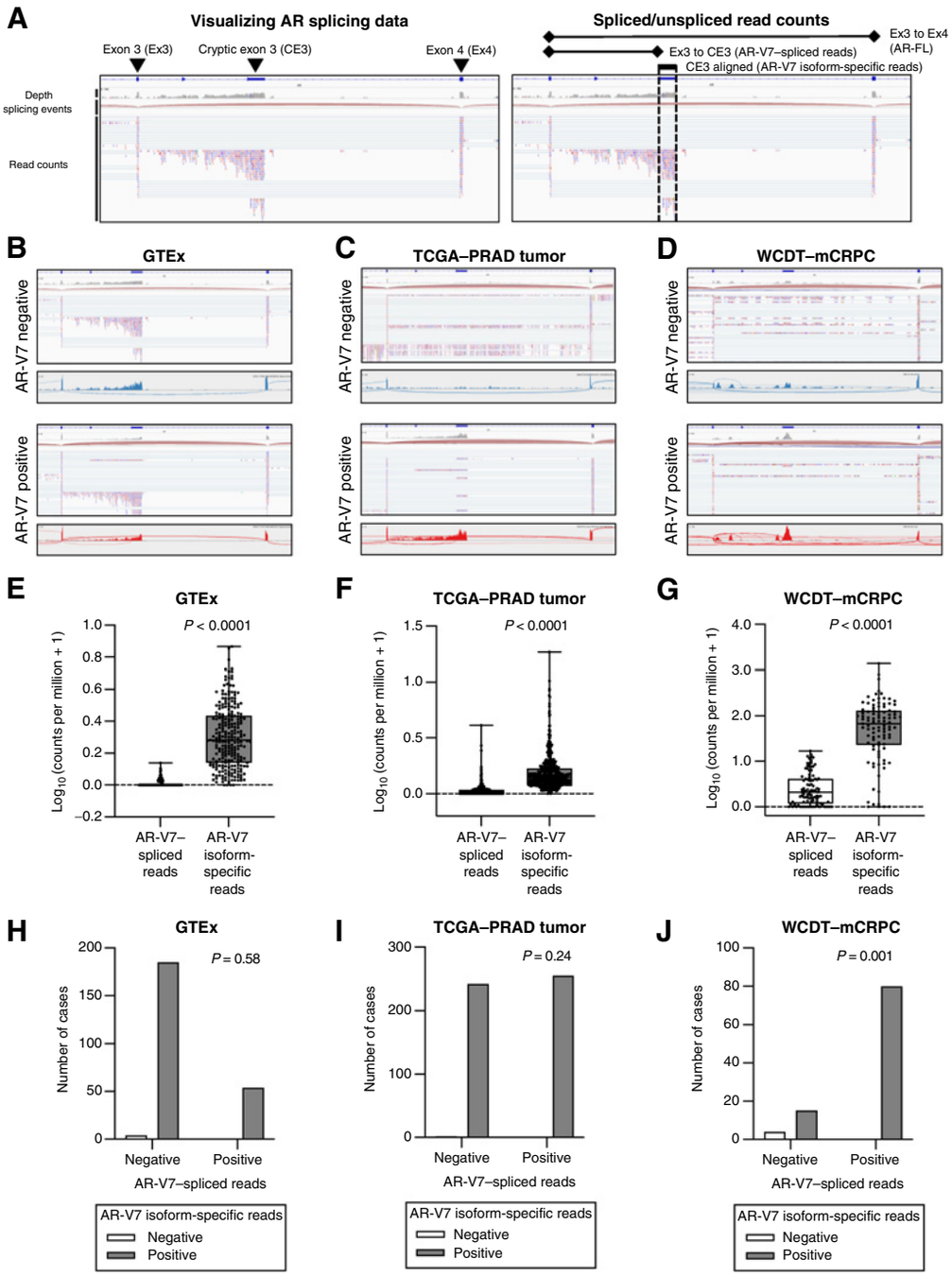

Figure 1.

Comparison of AR-V7 quantification in publicly available datasets. **A,** Screenshot of the Integrative Genomics Viewer (IGV) annotated with the information contained in each track with respect to specific regions of the *AR* locus (left) and splice junctions (right). **B–D,** Screenshots (as in **A**) and sashimi plots for cases from genotype-tissue expression (GTEx; **B**), The Cancer Genome Atlas–prostate adenocarcinoma tumor (TCGA–PRAD tumor; **C**) and West Coast Dream Team–metastatic CRPC (WCDT–mCRPC; **D**) cohorts. Representative cases of AR-V7–negative (blue) and AR-V7–positive (red) cases are shown as determined by the presence of splicing between exon 3 and cryptic exon 3 as shown in the red sashimi plots. **E–G,** For each case in the GTEx ($n = 243$; **E**), TCGA–PRAD tumor ($n = 499$; **F**), and WCDT–mCRPC ($n = 99$; **G**) cohorts, the number of read counts corresponding to AR-V7–spliced reads (between exon 3 and cryptic exon 3) and AR-V7 isoform–specific reads (aligning to cryptic exon 3, dashed vertical lines in **A**) are shown. Spliced reads data are shown as $\log_{10}$ (spliced reads per million + 1); isoform-specific read data are shown as $\log_{10}$ (read counts per million + 1). Statistical significance between differences was measured by Mann–Whitney tests. Box shows median and interquartile range; bars show minimum and maximum values. **H–J,** The number of cases showing concordance between the presence of AR-V7 isoform-specific reads and the presence of AR-V7–spliced reads is shown for GTEx (**H**), TCGA-PRAD tumor (**I**), and WCDT–mCRPC (**J**) cohorts. Statistical significance between associations was measured by two-sided Fisher exact tests.

aligned to the *AR-V7* isoform-defining cryptic exon 3 (CE3) in the intronic regions with reads between exons 3 (Ex3) and 4 (Ex4) of *AR* versus reads that were truly spliced from Ex3 to CE3 (**Fig. 1A**). When *AR-V7* status was defined by evidence of Ex3–CE3 splicing, reads aligning to CE3 were still observed in *AR-V7*–negative cases from the benign prostate genotype-tissue expression cohort (GTEx; $n = 243$), primary prostate adenocarcinoma cohort (TCGA–PRAD; $n = 499$), and the Stand Up 2 Cancer–Prostate Cancer Foundation West Coast Dream Team metastatic CRPC cohort (WCDT–mCRPC; $n = 99$; **Fig. 1B–D**; refs. 49–51). Patterns similar to GTEx were also observed in the 52 cases of normal adjacent tissue profiled in TCGA–PRAD (Supplementary Fig. S1A). As anticipated, Ex3–CE3-spliced reads were most abundant in the WCDT–mCRPC cohort (**Fig. 2A**), although across all four cohorts, CE3-aligned reads were significantly more abundant than Ex3–CE3-spliced reads (**Fig. 1E–G**; Supplementary Fig. S1B; $P < 0.0001$, Mann–Whitney test). This observation was not due to any apparent deficiency in splicing detection, as full-length *AR* (defined by splicing from Ex3–Ex4) was observed in all four cohorts (**Fig. 2B**). When normalized by the total number of reads mapped to the *AR* locus (**Fig. 2C**), the WCDT–mCRPC cohort maintained the highest abundance of *AR-V7*–spliced reads (**Fig. 2D**). Stratified by *AR-V7* status, only the WCDT–mCRPC cohort demonstrated a significant association between CE3-aligned reads and Ex3–CE3-spliced reads (**Fig. 1H–J**; Supplementary Fig. S1C; $P = 0.001$; Fisher exact test). We next applied a 59-gene AR-V7 signature score that we have previously shown to be associated with AR-V7 abundance across independent CRPC cohorts (14). Having derived this score from independent CRPC cohorts, we applied it to the WCDT–mCRPC cohort and demonstrated that *AR-V7*–positive patients had significantly ($P < 0.001$, Welch t test) higher AR-V7 signature scores than *AR-V7*–negative patients (**Fig. 2E**). Taken together, these important differences in the transcriptomic quantification of *AR-V7* abundance affect biomarker detection and suggest that the abundance of reads spanning the Ex3–CE3 splice junction is more accurate than CE3 read counts alone.

AR-V7 antibodies demonstrate differences in AR-V7 protein detection in untreated CS, but not CRPC

We have previously evaluated two AR-V7 antibodies for IHC, RevMAb RM7 (1 in 500, primary antibody dilution) and Abcam EPR15656 (1 in 200, primary antibody dilution) for the detection of AR-V7 protein in prostate cancer tissue biopsies (14, 41, 52). To directly compare these antibodies, we utilized CSPC biopsies, with matched CRPC biopsies, on which IHC by both antibodies had been performed previously (ICR/RMH matched CSPC and CRPC cohort; Supplementary Fig. S2 and Supplementary Table S1; refs. 14, 41, 52). IHC with RM7 on prostate cancer tissue biopsies demonstrated almost exclusively nuclear staining, whereas IHC with EPR15656 demonstrated both nuclear and cytoplasmic staining (**Fig. 3A**; refs. 12, 14, 41). Comparing both antibodies, nuclear AR-V7 staining significantly

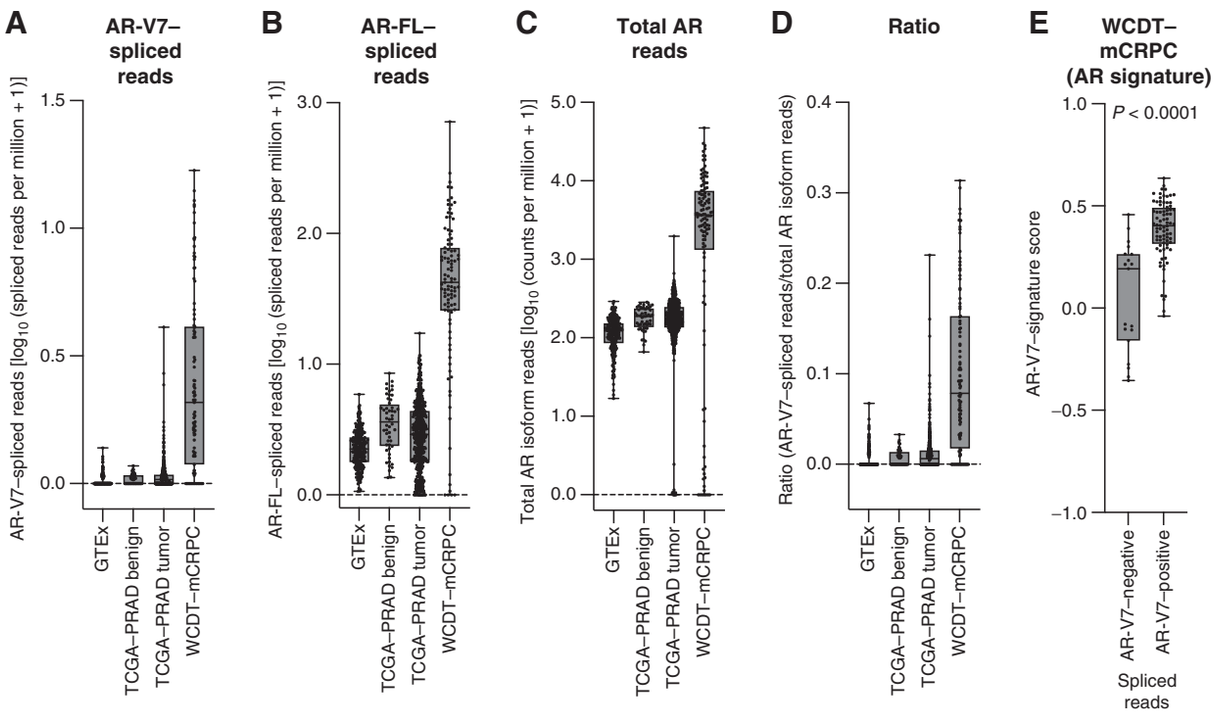

Figure 2.

Enumeration of AR isoforms and AR-V7 signature scores in publicly available data sets. **A–D,** The number of reads corresponding to AR-V7 (splicing between exon 3 and cryptic exon 3; **A**), full-length AR (AR-FL; splicing between exon 3 and exon 4; **B**), mapped to the AR locus (**C**), and AR-V7/AR-FL read count ratio (**D**) are shown for the GTEx ($n = 243$), TCGA–PRAD benign ($n = 52$), TCGA–PRAD tumor ($n = 499$), and WCDT–mCRPC ($n = 99$) cohorts. Spliced read data (**A–B**) are shown as $\log_{10}$ (spliced reads per million + 1), and isoform-specific read data (**C**) are shown as $\log_{10}$ (read counts per million + 1). Box shows median and interquartile range; bars show minimum and maximum values. **E,** AR-V7–signature score for AR-V7–negative and –positive patients determined by AR-V7–spliced reads in the WCDT–mCRPC cohort. Box shows median and interquartile range; bars show minimum and maximum values. Statistical significance between differences was measured by the Welch t test.

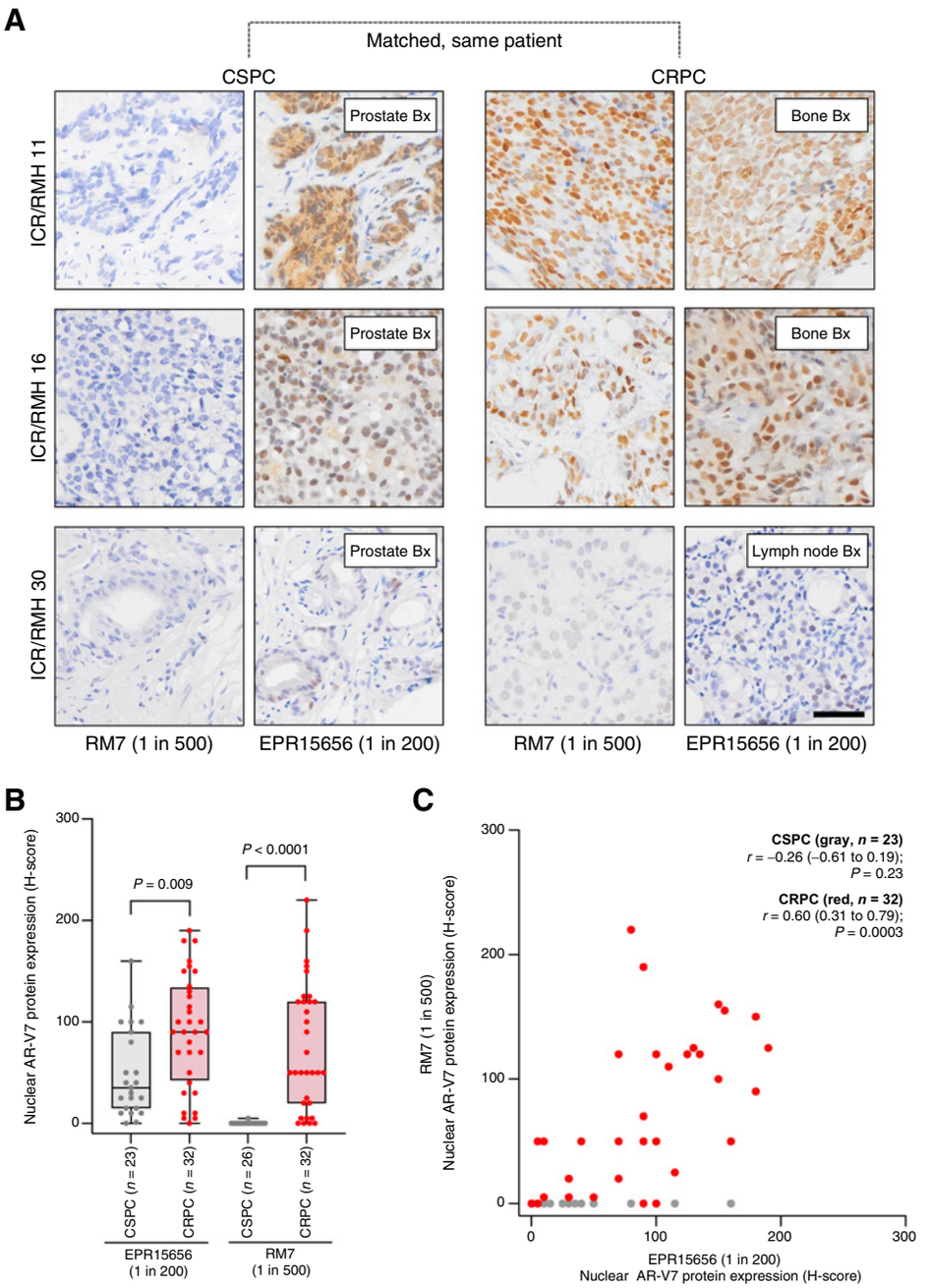

Figure 3.

AR-V7 protein quantification by two IHC assays in matched, same patient, castration-sensitive and castration-resistant prostate cancer tissue biopsies. **A,** Representative micrographs of AR-V7 protein detection by IHC using EPR15656 (Abcam, 1 in 200) and RM7 (RevMAb, 1 in 500) antibodies in three patients with matched CSPC and CRPC tissue biopsies from the Institute of Cancer Research/Royal Marsden Hospital (ICR/RMH) matched CSPC and CRPC cohort (scale bar: 50 μm). Prostate, lymph node, and bone biopsies (Bx) are shown. **B,** Nuclear AR-V7 staining (H-score) using EPR15656 (23 CSPC and 32 CRPC) and RM7 (26 CSPC and 32 CRPC) antibodies was determined. Box shows median and interquartile range; bars show minimum and maximum values. Statistical significance between differences was measured by Mann–Whitney tests. **C,** Nuclear AR-V7 staining (H-score) for EPR15656 and RM7 in the same 23 CSPC (gray) and 32 CRPC (red) biopsies is shown. Statistical significance between correlations was determined by Spearman rank.

increased (EPR15656, $P = 0.009$, Mann–Whitney test; RM7, $P < 0.0001$, Mann–Whitney test) from CSPC [EPR15656, median H-score 35, interquartile range (IQR) 15–90; RM7, H-score 0, IQR 0–0) to CRPC (EPR15656, H-score 90, IQR 42.5–133.8; RM7, H-score 50, IQR 20–120; **Fig. 3B**]. Similarly, using EPR15656, cytoplasmic AR-V7 staining significantly ($P = 0.03$, Mann–Whitney test) increased from CSPC (H-score 20, IQR 0–70) to CRPC (H-score 70, IQR 10–90; Supplementary Fig. S3). Conversely, and consistent with patterns of exclusively nuclear staining, no significant ($P > 0.99$, Mann–Whitney test) change in cytoplasmic staining between CSPC (H-score 0, IQR 0–0) and CRPC (H-score 0, IQR 0–0) was observed when using the RM7 antibody (Supplementary Fig. S3). Staining intensities demonstrated a significant correlation between nuclear AR-V7 staining by EPR15656 and RM7 antibodies in CRPC biopsies ($r = 0.60$, 0.31–0.79, $P = 0.0003$, Spearman rank) but not CSPC biopsies ($r = -0.26$; −0.61 to 0.19, $P = 0.23$, Spearman rank; **Fig. 3C**), highlighting an important difference in the performance of these antibodies to detect AR-V7 staining in untreated primary prostate cancer.

Analytical validation of AR-V7 antibodies for IHC demonstrates differences in specificity and detection of AR-V7 protein in multiple prostate cancer models

Having demonstrated differences between IHC by RM7 and EPR15656 in prostate cancer tissue biopsies, we next wanted to

interrogate further the sensitivity and specificity of both antibodies. We, therefore, performed IHC on FFPE pellets of multiple prostate cancer cell lines. Cell lines previously confirmed to express AR-V7 (LNCaP95, 22Rv1, and VCaP) were positive for AR-V7 by IHC with RM7, whereas AR-V7–negative cell lines (LNCaP, C42, DU145, PC3, and PNT2) were not positive (Supplementary Fig. S4A). Although LNCaP95, 22Rv1, and VCaP were also positive for AR-V7 by IHC with EPR15656, the AR-V7–negative cell lines PC3 and PNT2 demonstrated positivity for AR-V7 by IHC with EPR15656 indicative of nonspecific staining (Supplementary Fig. S4B). AR protein status was confirmed in all cell lines using both AR N-terminal (NTD) and C-terminal (CTD) antibodies, demonstrating no positivity for AR in PC3 and PNT2 cell lines (Supplementary Fig. S4C and S4D). In addition, western blotting with both RM7 and EPR15656 antibodies demonstrated a strong AR-V7 band at 80 kDa in LNCaP95, 22Rv1, and VCaP, but EPR15656 detected a nonspecific band in PC3 that was not detected by either AR-NTD or AR-CTD antibodies (Supplementary Fig. S5A–S5D). These data reinforce previous studies that demonstrate both RM7 and EPR15656 recognize AR-V7 protein but EPR15656 may have off-target liabilities that need to be considered (12, 14, 41).

We next performed IHC with both the RM7 and EPR15656 antibodies on VCaP and PDX mouse models. Two PDX models were derived from metastatic biopsies of prostate cancer patients with CRPC (Supplementary Fig. S6A–S6B). Once established in intact mice (CP50 and CP89), new castrate (designated C) PDX lines were developed and treated with vehicle or testosterone (20 mg/kg o.d.) for 7 days. RNA-seq analyses using Ex3–CE3-spliced reads to quantify *AR-V7* demonstrated an increased abundance of *AR-V7* mRNA in CP50 and CP89 in response to castration that was reversed by testosterone treatment (**Fig. 4A** and **B**). IHC by RM7 demonstrated a consistent increase in nuclear AR-V7 staining in tumors grown in intact mice (CP50IV, median H-score 0, range, 0–0; CP89IV, H-score 0; range, 0–0) compared with castrate mice (CP50CV, H-score 50; range, 40–50; CP89CV, H-score 17; range, 9–25), and this was suppressed by testosterone treatment (CP50CT, H-score 0; range, 0–0; CP89CT, H-score 0; range, 0–2; **Fig. 4A** and **B**). By contrast, IHC with EPR15656 demonstrated nuclear AR-V7 staining in tumors grown in intact mice where *AR-V7*–spliced RNA was very low or absent (CP50IV, H-score 135; range, 130–135; CP89IV, H-score 90; range, 20–95) and there was surprisingly little change when tumors were established in castrate mice (CP50CV, H-score 105, range, 45–110; CP89CV, H-score 80; range, 50–105), with minimal further change with testosterone treatment (CP50CT, H-score 100, range, 95–116; CP89CT, H-score 70, range, 27–107; **Fig. 4A** and **B**). In addition, cytoplasmic positivity was observed with EPR15656, but not with RM7 (**Fig. 4A** and **B**). Similar to the PDX's, staining with RM7 demonstrated an increase in nuclear AR-V7 staining in the VCaP mouse xenograft as it progressed from castration sensitive (H-score 0, range, 0–0) through castration resistance (H-score 105, range, 85–125) to abiraterone and enzalutamide resistance (H-score 175, range, 140–205; **Fig. 4C**). However, IHC with EPR15656 also demonstrated nuclear AR-V7 staining at the initial castration-sensitive stage (H-score 60; range, 40–165) with only modest increases in intensity with the development of castration resistance (H-score 120, range, 60–190) and abiraterone and enzalutamide resistance (H-score 110, range, 85–180; **Fig. 4C**). In addition, as with the PDX models, cytoplasmic positivity was again observed with EPR15656, but not with RM7 (**Fig. 4C**). These data further highlight the differences between IHC with RM7 and EPR15656 in clinically relevant models and demonstrate the dynamic nature of *AR-V7* mRNA and AR-V7 staining that may further complicate its use as a clinical biomarker.

We further performed additional IHC with RM7 on the LuCaP series of prostate cancer PDXs for which matched RNA-seq was also available. Although several CR subline models demonstrated an increased abundance of *AR-V7* mRNA, this was not observed in all PDXs (**Fig. 5A**; ref. 40). Independent IHC performed on these models at the ICR (1 in 500; **Fig. 5B**) and UW (1 in 50; **Fig. 5C**) confirmed an increase in nuclear AR-V7 staining in some, but not all, CR sublines, with more intense staining observed in the UW series. We observed a significant positive association between *AR-V7* mRNA (Ex3–CE3-spliced reads) and both nuclear AR-V7 staining by ICR RM7 IHC ($r =$ 0.64, 0.40–0.79, $P < 0.0001$, Spearman rank) and UW RM7 IHC ($r =$ 0.66, 0.44–0.81, $P < 0.0001$, Spearman rank; **Fig. 5D** and **E**). In addition, there was a significant positive association between ICR RM7 IHC and UW RM7 IHC ($r = 0.72$, 0.53–0.85, $P < 0.0001$, Spearman rank) staining (**Fig. 5F**). Furthermore, LuCaP PDX models that were AR-V7 positive as determined by *AR-V7*–spliced reads ($P = 0.0005$, Mann–Whitney), ICR RM7 IHC assay ($P = 0.0001$, Mann–Whitney), and UW RM7 IHC ($P = 0.0003$, Mann–Whitney) had significantly higher AR-V7 gene-expression signature scores than AR-V7–negative models (**Fig. 5A–C**). These data demonstrate that quantification of nuclear AR-V7 staining by the RM7 IHC, in two independent laboratories, is significantly associated with quantification of *AR-V7* mRNA by Ex3–CE3-spliced reads, and that these measures of AR-V7 quantification are associated with an AR-V7 signature score.

Having demonstrated that IHC by RM7 had more intense nuclear AR-V7 positivity at higher concentrations, and to increase potential sensitivity to detect AR-V7 protein in primary prostate cancer, we evaluated the sensitivity and specificity of IHC by RM7 and EPR15656 at various primary antibody concentrations in multiple FFPE pellets of prostate cancer cell lines (Supplementary Fig. S7A and S7B). IHC by RM7 remained specific at a 1 in 50 dilution, demonstrating positive and exclusively nuclear staining for AR-V7 protein in AR-V7–positive cell lines (LNCaP95, 22Rv1, and VCaP) and showed no staining in AR-V7–negative cell lines (LNCaP, C42, DU145, PC3, and PNT2; Supplementary Fig. S7A). However, we did identify nucleolar staining that is likely to be nonspecific in C42 cells at the 1 in 50 dilution, and thus did not evaluate higher concentrations of RM7 antibody. Although the IHC by EPR15656 demonstrated more intense nuclear AR-V7 positivity in AR-V7–positive cell lines at 1 in 50 dilution than in lower dilutions of this antibody, this intensity was also associated with reduced specificity and off-target positivity in nearly all AR-V7–negative cell lines (Supplementary Fig. S7B). These data confirm that EPR15656 has off-target IHC liabilities (12, 14, 41).

Assured of the robust sensitivity and specificity of IHC by RM7 at the 1 in 50 dilution, we stained the previously used VCaP and PDX (CP50 and CP89) models at this concentration. At 1 in 50 dilution, IHC by RM7 demonstrated more intense, exclusively nuclear staining, with an increase in nuclear AR-V7 staining from an intact state (CP50IV, median H-score 0, range, 0–0; CP89IV, H-score 5, range, 0–5) to a castrate state (CP50CV, H-score 70, range, 50–95; CP89CV, H-score 85, range, 40–90) that was suppressed by testosterone treatment (CP50CT, H-score 0, range, 0–0; CP89CT, H-score 0, range, 0–0; Supplementary Fig. S8A and S8B). We again observed an increase in nuclear AR-V7 staining in the VCaP mouse xenograft as it progressed from castration sensitive (H-score 0, range, 0–0) through castration resistance (H-score 150, range, 115–160) to abiraterone and enzalutamide resistance (H-score 180, range, 165–205; Supplementary Fig. S8C). Despite the increase in antibody concentration, there was

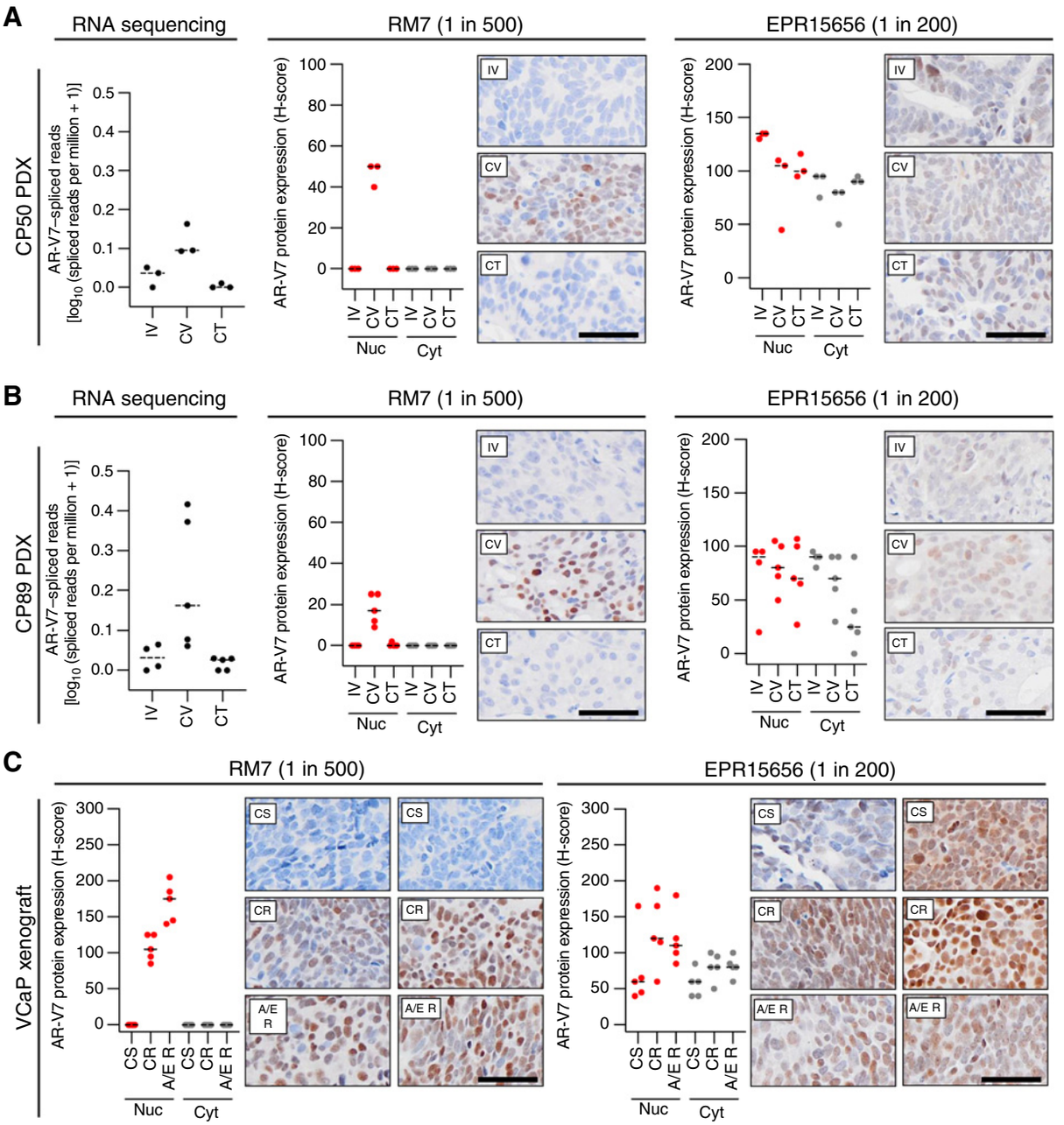

Figure 4.

Comparison of AR-V7 IHC assays, and AR-V7–spliced reads from RNA analysis, in the CP50 and CP89 prostate cancer PDX, and VCaP mouse xenograft, in response to hormonal manipulation. **A,** For CP50 prostate cancer PDX: intact CP50 was treated with vehicle for 7 days (IV, $n = 3$) and its castrate subline CP50C was treated with either vehicle (CV, $n = 3$) or 20 mg/kg testosterone daily (CT, $n = 3$) for 7 days and RNA-seq and IHC was performed. AR-V7–spliced reads (between exon 3 and cryptic exon 3) were determined from RNA-seq analysis. Spliced reads data are shown as $\log_{10}$ (spliced reads per million + 1). Representative micrographs of AR-V7 protein detection by IHC using EPR15656 (Abcam, 1 in 200) and RM7 (RevMAb, 1 in 500) antibodies are shown (scale bar: 50 μm). Nuclear and cytoplasmic AR-V7 staining (H-score) was determined. Line represents the median H-score. **B,** For CP89 prostate cancer PDX: intact CP89 was treated with vehicle for 7 days (IV, $n = 4$) and its castrate subline CP89C was treated with either vehicle (CV, $n = 5$) or 20 mg/kg testosterone daily (CT, $n = 5$) for 7 days and RNA-seq and IHC was performed. AR-V7 spliced reads (between exon 3 and cryptic exon 3) were determined from RNA-seq analysis. Spliced reads data are shown as $\log_{10}$ (spliced reads per million + 1). Representative micrographs of AR-V7 protein detection by IHC using EPR15656 (Abcam, 1 in 200) and RM7 (RevMAb, 1 in 500) antibodies are shown (scale bar: 50 μm). Nuclear and cytoplasmic AR-V7 staining (H-score) was determined. Line represents the median H-score. **C,** For VCaP mouse xenografts; samples were taken from tumors that were castration sensitive (CS; $n = 5$), as they progressed to castration resistant (CR; $n = 5$), and as resistance to abiraterone and enzalutamide developed (A/E R, $n = 5$), and IHC was performed. Representative micrographs of AR-V7 protein detection by IHC using EPR15656 (Abcam, 1 in 200) and RM7 (RevMAb, 1 in 500) antibodies are shown (scale bar: 50 μm). Nuclear and cytoplasmic AR-V7 staining (H-score) was determined. Line represents the median H-score.

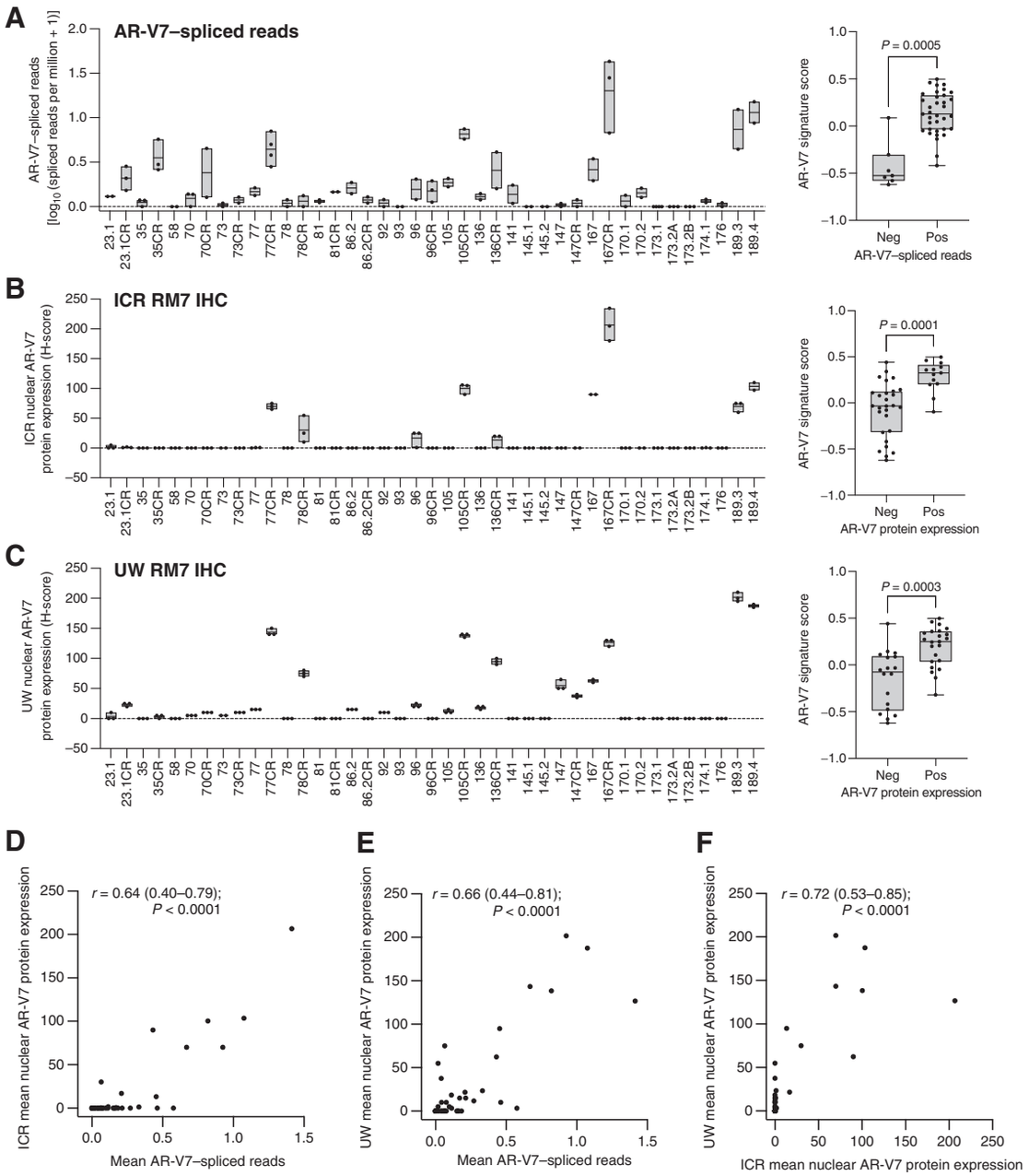

Figure 5.

Comparison of AR-V7 IHC assays between laboratories, and with AR-V7 spliced reads from RNA analysis, in the LuCaP series of prostate cancer PDX models. **A,** For each model in the LuCaP series, the number of read counts corresponding to AR-V7 spliced reads (between exon 3 and cryptic exon 3) was determined from RNA-seq analysis. Spliced reads data are shown as $\log_{10}$ (spliced reads per million + 1). Box shows mean and bars show minimum and maximum values. AR-V7 signature score shown for AR-V7–negative and –positive models determined by AR-V7–spliced reads. Box shows median and interquartile range; bars show minimum and maximum values. Statistical significance between differences were measured by the Welch *t* test. **B–C,** For each model in the LuCaP series nuclear AR-V7 staining (H-score) was determined by IHC using RM7 antibody and was performed at the ICR (1 in 500; **B**) and UW (1 in 50; **C**). Box shows mean and bars show minimum and maximum values. AR-V7 signature score shown for AR-V7–negative and –positive models determined by ICR and UW RM7 IHC. Box shows median and interquartile range; bars show minimum and maximum values. Statistical significance between differences were measured by the Welch *t* test. **D–E,** The association between mean AR-V7–spliced reads and mean nuclear AR-V7 staining determined at ICR (**D**) and UW (**E**) is shown. Statistical significance between correlations was determined by Spearman rank. **F,** The association between mean nuclear AR-V7 staining determined at ICR and UW is shown. Statistical significance between correlations was determined by Spearman rank.

no cytoplasmic staining seen in all models (Supplementary Fig. S8A–S8C). These data further highlight that nuclear AR-V7 staining by RM7 IHC is associated with quantification of AR-V7 mRNA by Ex3–CE3-spliced reads.

Validated AR-V7 IHC rarely identifies AR-V7 protein in primary prostate cancer and detection does not associate with clinical outcome

We next explored both IHC with RM7 at 1 in 50 dilution, and EPR15656 at 1 in 200 dilution, in two independent patient cohorts of primary advanced prostate cancer (ICR/RMH primary advanced cohort) and primary localized prostate cancer (UW primary localized cohort) to determine whether AR-V7 protein was identified and associated with clinical response (Supplementary Fig. S9; Supplementary Tables S2 and S3). The ICR/RMH primary advanced cohort comprised of 22 patients who received systemic therapy for primary advanced prostate cancer; only 2 patients (9%) demonstrated nuclear AR-V7 staining, and no patient demonstrated cytoplasmic positivity when tissues were evaluated with RM7 IHC (**Fig. 6A** and **B**). Nuclear AR-V7 staining at baseline did not associate with time to the development of CRPC ($r = -0.16$; −0.56 to 0.29, $P = 0.47$, Spearman rank) or overall survival ($r = -0.24$; −0.61 to 0.22, $P = 0.29$, Spearman rank; **Fig. 6C** and **D**). By contrast, IHC by EPR15656 identified AR-V7 positivity in primary advanced prostate cancer, with 15 patients (68%) demonstrating nuclear AR-V7 staining, and 6 patients (27%) demonstrating cytoplasmic positivity (**Fig. 6A** and **B**). Despite increased

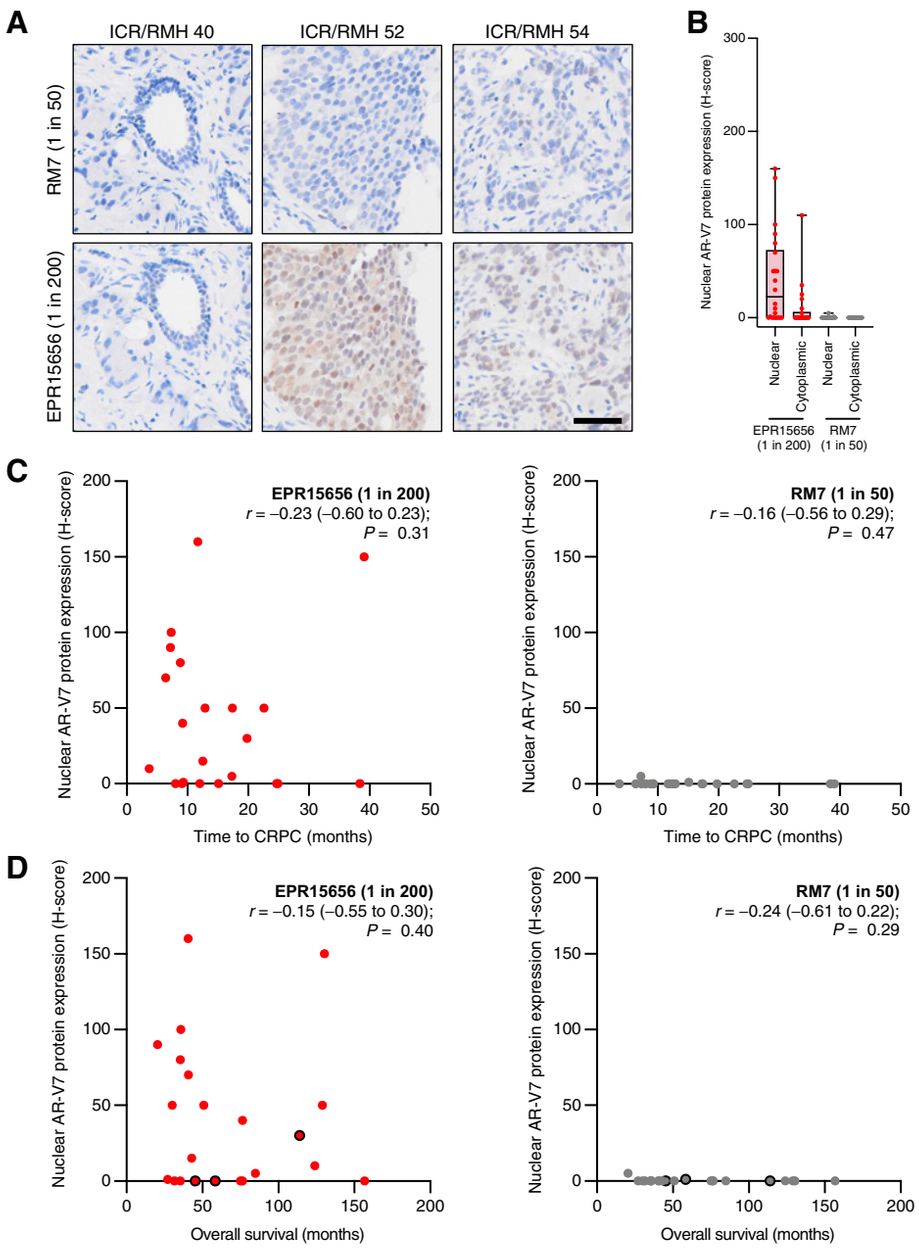

Figure 6.
AR-V7 protein quantification by two IHC assays in diagnostic biopsies of prostate cancer patients who received systemic therapy alone. **A,** Representative micrographs of AR-V7 protein detection by IHC using EPR15656 (Abcam, 1 in 200) and RM7 (RevMAb, 1 in 50) antibodies in three diagnostic CSPC prostate biopsies from patients in the Institute of Cancer Research/Royal Marsden Hospital (ICR/RMH) primary advanced cohort (scale bar: 50 μm). **B,** Nuclear and cytoplasmic AR-V7 staining (H-score) using EPR15656 (Abcam, 1 in 200, red circles) and RM7 (RevMAb, 1 in 50, gray circles) antibodies was determined. Box shows median and interquartile range; bars show minimum and maximum values. **C,** Association between nuclear AR-V7 staining (H-score) using EPR15656 (EPR15656, 1 in 200, red circles) and RM7 (RevMAb, 1 in 50, gray circles) antibodies and time to CRPC (months) from diagnosis is shown. Statistical significance between correlations were determined by Spearman rank. **D,** Association between nuclear AR-V7 staining (H-score) using EPR15656 (EPR15656, 1 in 200, red circles) and RM7 (RevMAb, 1 in 50, gray circles) antibodies and overall survival (months) from diagnosis is shown. Three patients remain alive at last follow-up (black circle outline). Statistical significance between correlations was determined by Spearman rank.

nuclear AR-V7 staining, there remained no association between nuclear AR-V7 staining at baseline and time to development of CRPC ($r = -0.23$; -0.60 to 0.23, $P = 0.31$, Spearman rank) or overall survival ($r = -0.15$; -0.55 to 0.30, $P = 0.40$; Spearman rank; **Fig. 6C** and **D**).

This pattern of staining was further validated in the UW primary localized cohort, which consisted of 26 prostatectomies with benign prostate and prostate cancer tissue, and other benign tissue (including kidney, spleen, and salivary gland; Supplementary Fig. S9 and Supplementary Table S3). The prostate cancer tissues from these prostatectomies were included in the 295 samples previously studied with the RM7 antibody (14). We observed no nuclear AR-V7 staining in prostatic adenocarcinoma tumor (H-score 0, IQR 0–0; ref. 14). In addition, further to previous studies, we demonstrate no nuclear AR-V7 positivity in adjacent benign prostate tissue (median H-score 0, IQR 0–0) or other benign tissues (H-score 0, IQR 0–0; Supplementary Fig. S10). Although IHC by EPR15656 demonstrated less nuclear AR-V7 staining in this cohort, reactivity was observed even in benign prostate (median H-score 2, IQR 0–4.5), prostate tumor (H-score 0, IQR 0–1), and other benign tissues (H-score 1, IQR 0–4; Supplementary Fig. S10). These data confirm that IHC by RM7 very rarely detects nuclear AR-V7 staining in both advanced and localized primary prostate cancer tissues at diagnosis, and although positivity is seen with IHC by EPR15656 in primary prostate cancer and other tissue types, this is likely to be related to its off-target liabilities, with EPR15656 staining not associated with clinical outcomes in this patient cohort.

AR-V7 mRNA quantification by junction-specific reads does not increase in response to neoadjuvant therapy or predict response to therapy in primary prostate cancer

Finally, we assessed whether AR-V7 can predict or mediate resistance to short-course intense ADT prior to prostatectomy, using tissue samples and RNA-seq data from a recent clinical trial at the U.S. NCI (53). As RNA was extracted from FFPE samples, we first sought to determine whether our ability to detect spliced and total *AR* was affected by these processing steps, using a localized prostate cancer cohort (Supplementary Table S4 and Supplementary Fig. S11A; $n = 84$) of matched benign and tumor blocks subjected to whole transcriptome sequencing. *AR-V7* abundance in both the benign and tumor blocks was comparable with the GTEx and TCGA–PRAD benign and tumor tissues (see **Fig. 2A**) except for a single case that received a short course of bicalutamide prior to prostatectomy (**Fig. 7A**). The NCI neoadjuvant cohort (Supplementary Table S5 and Supplementary Fig. S11B; $n = 37$) similarly showed extremely low levels of Ex3–CE3 *AR-V7*–spliced reads in matched pre- and posttreatment specimens (**Fig. 7B**). Moreover, this low abundance of spliced reads observed in biopsy specimens did not track with treatment response as measured by the volume of residual disease after therapy (**Fig. 7B**). This finding was not due to a deficiency in detecting splicing events by RNA-seq, as both cohorts demonstrated comparable levels of full-length AR (Ex3–Ex4 splicing) to TCGA–PRAD (Supplementary Fig. S12).

In addition to the transcriptomic analysis performed, all posttreatment specimens were evaluated for residual tumor using both full-length AR and RM7 AR-V7 antibodies by IHC. As depicted in **Fig. 7C**, the most common observation was the restoration of nuclear AR expression in large volumes of residual tumor (blue shading) with microscopic nests of cells demonstrating rare AR-V7 staining. All posttreatment samples had H-scores less than 10 (**Fig. 7D**). Despite a range of residual tumor volumes after therapy, neither AR-V7–spliced reads nor nuclear AR-V7 staining tracked with residual tumor volume, indicating that AR-V7 levels neither predict nor track with residual tumor volume following neoadjuvant therapy in this clinical study (**Fig. 7E** and **F**).

Discussion

The AR remains the major therapeutic target in CRPC (3). AR-targeted therapies have improved the overall survival and quality of life of patients with CRPC (2, 3). However, acquired resistance to AR-targeting therapies is common and is associated with the emergence of AR-V7, a constitutively active AR splice variant at the mRNA and protein levels (9–14, 18, 41, 54). More recently, AR-V7 status as a predictive biomarker has shown clinical utility in guiding treatment with AR-targeted therapy versus systemic chemotherapy in assays featuring AR-V7 mRNA or protein reactive circulating tumor cells (CTC; refs. 9–13). However, the development of AR-V7 as a predictive biomarker in CRPC has not been without its challenges. These include (i) antibody specificity for AR-V7 protein in tissue samples; (ii) biomarker absence (CTC negative) being deemed AR-V7 negative; (iii) CTC enumeration potentially confounding survival analysis; (iv) confirming predictive over prognostic utility; and (v) limited translation to routine clinical care (10–14, 19–24, 41, 54).

The treatment landscape for advanced prostate cancer is rapidly changing with the demonstration that AR-targeting therapies improve the overall survival for patients with advanced CSPC, raising the question of whether AR-V7 may serve as a predictive biomarker earlier in the prostate cancer paradigm (3). However, the evidence supporting AR-V7 as a biomarker in CSPC has been associated with significant challenges that impact its clinical qualification. As shown here and by others, these challenges include the low abundance or absence of AR-V7 in CSPC, CSPC's high response rate to primary therapy including AR-targeting agents, and the complexity of multimodal treatment strategies being utilized earlier in the disease course (36). Nonetheless, multiple studies have reported that AR-V7 protein expression was associated with poorer outcomes in CSPC (31–35). An important consideration for these studies, and any tissue-based IHC analyses, is the analytical validation to determine the specificity and sensitivity of the antibodies used, which have mainly been RM7 and EPR15656 described in this study (14, 32, 34, 35).

Based on our head-to-head analyses here, and previously, IHC by EPR15656 recognizes AR-V7 protein but also clearly demonstrates nonspecificity with cross-reactivity with other undefined proteins in multiple orthogonal validation assays when compared with IHC by RM7 (14). This highlights the importance of careful antibody validation and the use of rigorous controls when new IHC assays are developed and applied (55–57). In addition, although AR-V7 staining by RM7 and EPR15656 antibodies significantly correlated in CRPC tissue biopsies, IHC by EPR15656 commonly showed AR-V7 reactivity in independent tissue cohorts of locally advanced primary prostate cancer, as well as in benign prostate and other benign tissues, compared with IHC by RM7. Furthermore, AR-V7 reactivity by either antibody did not associate with clinical outcomes in advanced primary prostate cancer treated with systemic therapy alone. Although it is possible that this increased AR-V7 reactivity in primary prostate cancer tissue samples seen with EPR15656 is due to superior sensitivity when compared with RM7, when considering the extensive validation shown here this is highly unlikely to be the case. These data indicate that this detected staining with EPR15656 in CSPC is largely likely to be a consequence of nonspecific cross-reactivity which may be further compounded by the varying preanalytical variables associated with archival tissues when used (57, 58).

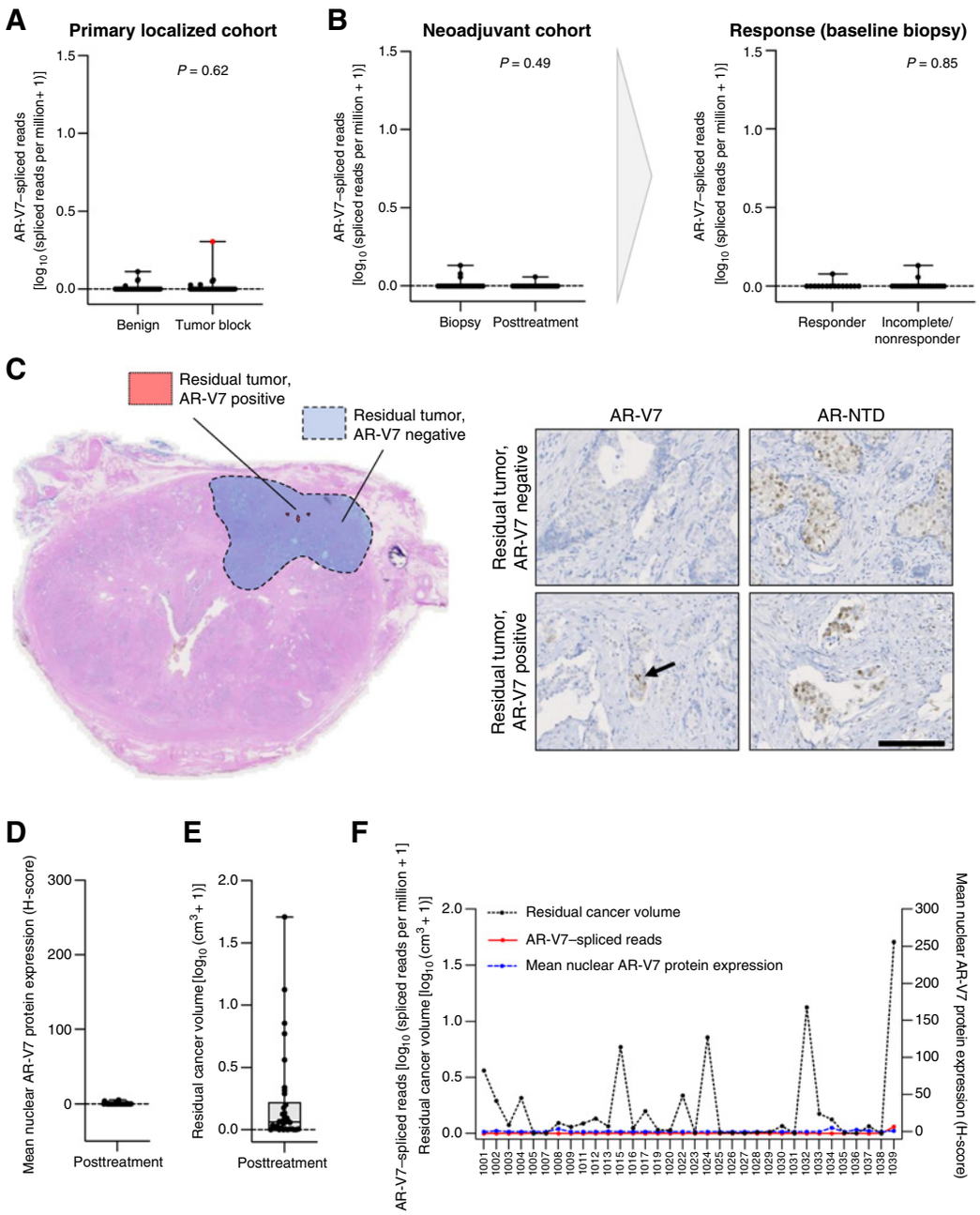

Figure 7.

AR-V7 quantification in prostate cancer patients who had primary radical prostatectomy or were treated with neoadjuvant ADT plus enzalutamide for locally advanced disease prior to prostatectomy. **A,** AR-V7–spliced reads [depicted as $\log_{10}$ (spliced reads per million + 1)] from 84 cases treated by radical prostatectomy. The red dot indicates the only case that received short-course neoadjuvant bicalutamide. Box shows median and interquartile range; bars show minimum and maximum values. Statistical significance between differences were measured by the Mann–Whitney test. **B,** AR-V7–spliced reads [depicted as $\log_{10}$ (spliced reads per million + 1)] from 37 cases treated with six months of neoadjuvant ADT plus enzalutamide prior to radical prostatectomy. Left, comparison of AR-V7–spliced reads from baseline biopsy and posttreatment. Right, stratification of baseline biopsies based on pathologic outcome of responder ($n = 15$) or incomplete/nonresponder ($n = 22$). **C,** Left, whole-slide imaging of a radical prostatectomy specimen from a representative incomplete/nonresponder; region of residual tumor is marked by a dotted line. Serial whole-slide section of AR-V7 staining using the RM7 (RevMAb, 1 in 100) antibody to identify regions of residual tumors that are AR-V7 positive (small foci marked in red) or AR-V7 negative (larger region marked in blue). Right, representative micrographs of AR-V7 and AR N-terminal (AR-NTD) IHC of residual tumor from serial sections (scale bar: 200 μm). **D,** Distribution of H-scores for AR-V7 IHC from posttreatment specimens with residual tumor ($n = 34$). **E,** Distribution of residual cancer volumes for each patient receiving six months of neoadjuvant ADT plus enzalutamide prior to radical prostatectomy. Data, $\log_{10}$ ($cm^3 + 1$). **F,** Overlay of data presented in **B**, **D,** and **E**, displayed by patient with all data available ($n = 34$). AR-V7–spliced read abundance and residual cancer volume are plotted on the left Y axis, and mean H-score for nuclear AR-V7 staining is plotted on the right Y axis.

An alternative to IHC is the quantification of segments of *AR-V7* mRNA that are specific to the isoform, using either RNA-seq or quantitative PCR. Here, utilizing multiple publicly available RNA-seq data sets, we, as have others, demonstrate that *AR-V7* mRNA is commonly identified in benign prostate and primary prostate cancer tissue using isoform-specific, CE3-aligned, reads (47). Studies have demonstrated that isoform-specific reads are significantly associated with, but are much more abundant than, Ex3-CE3–spliced reads (47). Consistent with this, *AR-V7* mRNA was much less frequently observed in benign prostate and primary prostate cancer tissue when Ex3–CE3-spliced reads were examined, with an expected significant increase in *AR-V7* abundance seen in metastatic CRPC. High levels of *AR* expression and the uncoupling of transcription with splicing in prostate cancer may explain in part the abundance of unspliced reads mapping to CE3 that we and others have reported in CSPC. These results may be a result of differential interpretation when using RNA-seq or quantitative PCR methods that do not measure across splice junctions (59). Taken together, reliable approaches for detecting AR-V7 mRNA and protein in CRPC demonstrate that AR-V7 expression is low, and does not associate with clinical outcomes in untreated primary prostate cancer.

It is important to carefully consider the limitations of the study presented. The major focus of this study was to analytically validate assays to quantify AR-V7 mRNA and protein in primary prostate cancer. Although multiple independent CSPC cohorts were studied, one limitation is the small number of patients across these cohorts. However, it is important to note that we have previously studied RM7 in over 350 CSPC cases, across institutions, with only a single patient being clearly positive for nuclear AR-V7 staining (14). As the treatment paradigm of primary prostate cancer changes with the addition of life-prolonging therapies (such as novel hormonal agents and/or docetaxel chemotherapy) to ADT, it may seem attractive to explore nuclear AR-V7 staining as a negative predictive biomarker (3). However, although these other studies were comprised of large prospective clinical cohorts, we have demonstrated that nuclear AR-V7 staining is rare in CSPC, and the absence of nuclear AR-V7 staining is unlikely to qualify clinically as a predictive biomarker to support patient stratification in primary prostate cancer, even in larger cohorts (3, 14). As there are currently no therapies that target AR-V7 specifically, AR-V7 remains a negative predictive biomarker for AR-directed therapies in CRPC (*i.e.*, positive AR-V7 staining does not predict favorable responses to any therapeutic agent). This is in sharp contrast to other molecular aberrations that have been shown to be positive predictive biomarkers in CRPC, such as DNA repair defects and PTEN loss, for PARP and AKT inhibition, respectively (10, 60, 61). Similar to the use of AR-directed therapies in CSPC, these novel agents may soon be utilized in CSPC to deliver durable interventions.

Despite our efforts to perform rigorous analytical validation in this study, an additional limitation is that it remains challenging to propose or recommend a standard protocol for IHC by RM7. Independent validation by each individual laboratory, using appropriate controls to limit pre- and postanalytical variables, is critical for developing any assay for tissue analyses such as these (57, 58). Thus, assays that quantify AR-V7 in CSPC will need to be subject to intense analytical validation before they can be considered for further clinical qualification of AR-V7 as a predictive biomarker in untreated primary prostate cancer, although our data would suggest that AR-V7 testing is unlikely to have a major role to play as a predictive biomarker in this setting. Finally, our finding that nuclear AR-V7 staining is rarely seen following neoadjuvant endocrine therapy in prostatectomy samples suggests that CSPC and CRPC biology differs with respect to AR-V7 emergence. However, it is important to acknowledge the challenges of the low tumor cell content in a subset of these samples, and further orthogonal validation in similar clinical cohorts is needed (53).

One additional unanswered question, that is likely to be of therapeutic importance, is what causes AR-V7 expression in CRPC. In clinical trials of neoadjuvant-intense ADT (using abiraterone or enzalutamide) in CSPC, these agents were not sufficient to induce significant AR-V7 expression after six months of therapy, even in patients with significant volumes of residual disease (62). We have further confirmed this in an independent cohort of patients who received neoadjuvant ADT and enzalutamide prior to radical prostatectomy, demonstrating low Ex3–CE3 *AR-V7*–spliced read abundance in matched pre- and posttreatment specimens (53). In addition, *AR-V7*–spliced reads did not associate with the volume of residual disease following therapy, and meticulous histopathologic analysis of residual disease demonstrated very rare AR-V7 staining. However, it is also important to note the challenges of low tumor cell content following endocrine therapy when performing these analyses. Furthermore, although AR-V7 protein expression is very rare and does not associate with residual tumor volume following neoadjuvant therapy, it is important to consider that it may be of biological importance in those cases where it is identified with robustly validated assays, and this warrants further investigation. In contrast to CSPC, approximately 30% of men with CRPC progressing on abiraterone or enzalutamide show detectable AR-V7 by CTC analysis, and much higher levels of AR-V7 reactivity are seen by tissue biopsy analysis following abiraterone and/or enzalutamide therapy (10, 14). Consistent with this, we show that the majority of PDX models developed from CRPC tissue biopsies demonstrate low/no AR-V7 mRNA or protein expression when grown in intact mice with a substantial increase in AR-V7 mRNA and protein abundance when castrate sublines are developed, which is reversed with testosterone treatment. These data indicate that CRPC biology supports the expression of AR-V7 mRNA and protein, but may also suggest that CSPC biology may differ with regard to induction of AR-V7 generation. Although not fully understood, these observations may be driven by the duration of treatment (six months versus years of androgen deprivation), reactivation of AR activity to produce a rising PSA (which is not observed after six months of neoadjuvant therapy), the emergence of *AR* structural variants in CRPC such as gene and enhancer amplifications, and expression of critical cofactors (14, 62–65). A better understanding of the mechanisms that drive the emergence of AR-V7 expression in prostate cancer may provide critical insight into prostate cancer biology and support novel treatment approaches.

Overall, our study highlights the challenges of developing analytically validated and clinically qualified predictive biomarkers for prostate cancer medicine. We demonstrate that AR-V7 mRNA and protein abundance is low in CSPC prior to treatment using robustly validated assays pursuing both IHC- and RNA-seq–based approaches. Similar efforts are needed for emerging assays for the detection of AR-V7 using CTCs and circulating cell-free RNA assays. Standardized controls, as well as stringent laboratory methods, are critical for both robust research discovery and determining clinical benefit. It remains to be seen whether AR-V7 can be validated and transferred to routine clinical care as a predictive biomarker in CSPC, and it may be that the true clinical importance of AR-V7 may only be realized with the development of therapies that specifically target AR-V7 and convert it from a negative predictive to the positive predictive biomarker.

Authors' Disclosures

C.T. Sprenger reports grants from NIH during the conduct of the study. S.P. Balk reports grants from the Prostate Cancer Foundation and NIH during the conduct of the study. E. Corey reports grants from Janssen Research and Development, Bayer Pharmaceuticals, Kronos Bio, Forma Therapeutics, Foghorn, Macrogenics, and AstraZeneca outside the submitted work. P.S. Nelson reports personal fees from Janssen, Bristol Myers Squibb, and Pfizer outside the submitted work. J.S. de Bono reports grants and personal fees from Amgen, Astellas, Bayer, Bioxcel Therapeutics, Boehringer Ingelheim, Cellcentric, Daiichi, Eisai, Genentech/Roche, Genmab, GSK, Harpoon, ImCheck Therapeutics, Janssen, Merck Serono, Merck Sharp & Dohme, Menarini/Silicon Biosystems, Orion, Pfizer, Qiagen, Sanofi Aventis, Sierra Oncology, Taiho, Terumo, and Vertex Pharmaceuticals outside the submitted work; in addition, J.S. de Bono is an employee of the ICR, which has received funding or other support for his research work from AstraZeneca, Astellas, Bayer, Cellcentric, Daiichi, Genmab, GSK, Janssen, Merck Serono, MSD, Menarini/Silicon Biosystems, Orion, Sanofi Aventis, Sierra Oncology, Taiho, Pfizer, and Vertex, and which has a commercial interest in abiraterone, PARP inhibition in DNA repair–defective cancers, and PI3K/AKT pathway inhibitors (no personal income). J.S. de Bono has a patent for DNA repair defects PARP issued but does not receive royalties (ICR-owned patent), as well as a patent for abiraterone acetate issued but does not receive royalties (ICR-owned patent); in addition, J.S. de Bono was named as an inventor, with no financial interest, for patent 8,822,438, submitted by Janssen, that covers the use of abiraterone acetate with corticosteroids. J.S. de Bono has been the CI/PI of many industry-sponsored trials. No disclosures were reported by the other authors.

Authors' Contributions

A.G. Sowalsky: Conceptualization, resources, data curation, formal analysis, supervision, funding acquisition, validation, investigation, visualization, methodology, writing–original draft, project administration, writing–review and editing. **I. Figueiredo:** Formal analysis, investigation. **R.T. Lis:** Formal analysis. **I. Coleman:** Software, formal analysis, validation, investigation, writing–review and editing. **B. Gurel:** Formal analysis, investigation. **D. Bogdan:** Formal analysis, investigation. **W. Yuan:** Formal analysis, funding acquisition. **J.W. Russo:** Formal analysis, investigation, writing–review and editing. **J.R. Bright:** Investigation. **N.C. Whitlock:** Investigation. **S.Y. Trostel:** Investigation. **A.T. Ku:** Formal analysis. **R.A. Patel:** Investigation, writing–review and editing. **L.D. True:** Resources, methodology. **J. Welti:** Investigation. **J.M. Jimenez-Vacas:** Formal analysis, investigation. **D.N. Rodrigues:** Formal analysis, investigation. **R. Riisnaes:** Formal analysis, investigation. **A. Neeb:** Formal analysis, investigation. **C.T. Sprenger:** Investigation. **A. Swain:** Investigation. **S. Wilkinson:** Investigation. **F. Karzai:** Investigation. **W.L. Dahut:** Resources, funding acquisition. **S.P. Balk:** Supervision, funding acquisition, writing–review and editing. **E. Corey:** Resources, formal analysis, investigation, writing–review and editing. **P.S. Nelson:** Resources, supervision, writing–review and editing. **M.C. Haffner:** Formal analysis, investigation, methodology, writing–review and editing. **S.R. Plymate:** Conceptualization, resources, formal analysis, supervision, investigation, methodology, writing–review and editing. **J.S. de Bono:** Resources, formal analysis, supervision, funding acquisition, investigation, project administration, writing–review and editing. **A. Sharp:** Conceptualization, data curation, formal analysis, supervision, validation, investigation, visualization, methodology, writing–original draft, project administration, writing–review and editing.

Acknowledgments

The authors gratefully acknowledge the patients and the families of patients who contributed to this study. This work was supported by Prostate Cancer UK (Travelling Prize Fellowship to J.M. Jimenez-Vacas; Research Funding to J.S. de Bono), the Prostate Cancer Foundation (Young Investigator Awards to S. Wilkinson, A.T. Ku, J.W. Russo, F. Karzai, A. Sharp; Challenge Awards to S.P. Balk, P.S. Nelson., J.S. de Bono, A. Sharp), the Intramural Research Program of the NIH, NCI, the Movember Foundation through the London Movember Centre of Excellence (CEO13 2-002 to J.S. de Bono), the Congressionally Directed Medical Research Program Prostate Cancer Research Program (Early Investigator Research Award to J.W. Russo; Translational Science Award to S.R. Plymate; Transformative Impact Award to L.D. True), the Wellcome Trust (Clinical Research Career Development Fellowship to A. Sharp), the NIHR Biomedical Research Centre, Cancer Research UK (Centre Programme and Experimental Cancer Medicine Centre grants to J.S. de Bono), the UK Department of Health, Biomedical Research Centre funding to the Royal Marsden, the Doris Duke Charitable Foundation (Clinical Scientist Development Award to M.C. Haffner), the V Foundation (V Scholar Grant to M.C. Haffner), the NIH (P50 CA090381 to S.P. Balk, C.T. Sprenger, P.S. Nelson; P50 CA097186 and R01 CA234715 to P.S. Nelson), the Veterans Affairs Research and Development Service (VA BLRD 2101BX003324 to S.R. Plymate), and the Lopker Family Foundation (to S.R. Plymate). Portions of this work utilized the computational resources of the NIH HPC Biowulf cluster. The establishment and characterization of the LuCaP patient-derived xenograft models were supported by the NIH (P50 CA097186 and P01 CA163227) and the Institute for Prostate Cancer Research (IPCR).

The publication costs of this article were defrayed in part by the payment of publication fees. Therefore, and solely to indicate this fact, this article is hereby marked "advertisement" in accordance with 18 USC section 1734.

Note

Supplementary data for this article are available at Clinical Cancer Research Online (http://clincancerres.aacrjournals.org/).

Received March 16, 2022; revised May 17, 2022; accepted June 8, 2022; published first June 10, 2022.

References

1. Culp MB, Soerjomataram I, Efstathiou JA, Bray F, Jemal A. Recent global patterns in prostate cancer incidence and mortality rates. Eur Urol 2020;77:38–52.
2. Sartor O, de Bono JS. Metastatic prostate cancer. N Engl J Med 2018;378:1653–4.
3. Westaby D, Fenor de La Maza MLD, Paschalis A, Jimenez-Vacas JM, Welti J, de Bono J, et al. A new old target: androgen receptor signaling and advanced prostate cancer. Annu Rev Pharmacol Toxicol 2022;62:131–53.
4. Conteduca V, Wetterskog D, Sharabiani MTA, Grande E, Fernandez-Perez MP, Jayaram A, et al. Androgen receptor gene status in plasma DNA associates with worse outcome on enzalutamide or abiraterone for castration-resistant prostate cancer: a multi-institution correlative biomarker study. Ann Oncol 2017;28:1508–16.
5. Kumar A, Coleman I, Morrissey C, Zhang X, True LD, Gulati R, et al. Substantial interindividual and limited intraindividual genomic diversity among tumors from men with metastatic prostate cancer. Nat Med 2016;22:369–78.
6. Linja MJ, Savinainen KJ, Saramaki OR, Tammela TL, Vessella RL, Visakorpi T. Amplification and overexpression of androgen receptor gene in hormone-refractory prostate cancer. Cancer Res 2001;61:3550–5.
7. Robinson D, Van Allen EM, Wu YM, Schultz N, Lonigro RJ, Mosquera JM, et al. Integrative clinical genomics of advanced prostate cancer. Cell 2015;161:1215–28.
8. Romanel A, Gasi Tandefelt D, Conteduca V, Jayaram A, Casiraghi N, Wetterskog D, et al. Plasma AR and abiraterone-resistant prostate cancer. Sci Transl Med 2015;7:312re10.
9. Antonarakis ES, Lu C, Luber B, Wang H, Chen Y, Zhu Y, et al. Clinical significance of androgen receptor splice variant-7 mRNA detection in circulating tumor cells of men with metastatic castration-resistant prostate cancer treated with first- and second-line abiraterone and enzalutamide. J Clin Oncol 2017;35:2149–56.
10. Armstrong AJ, Halabi S, Luo J, Nanus DM, Giannakakou P, Szmulewitz RZ, et al. Prospective multicenter validation of androgen receptor splice variant 7 and hormone therapy resistance in high-risk castration-resistant prostate cancer: the PROPHECY study. J Clin Oncol 2019;37:1120–9.
11. Scher HI, Graf RP, Schreiber NA, Jayaram A, Winquist E, McLaughlin B, et al. Assessment of the validity of nuclear-localized androgen receptor splice variant 7 in circulating tumor cells as a predictive biomarker for castration-resistant prostate cancer. JAMA Oncol 2018;4:1179–86.
12. Scher HI, Graf RP, Schreiber NA, McLaughlin B, Lu D, Louw J, et al. Nuclear-specific AR-V7 protein localization is necessary to guide treatment selection in metastatic castration-resistant prostate cancer. Eur Urol 2017;71:874–82.
13. Scher HI, Lu D, Schreiber NA, Louw J, Graf RP, Vargas HA, et al. Association of AR-V7 on circulating tumor cells as a treatment-specific biomarker with

outcomes and survival in castration-resistant prostate cancer. JAMA Oncol 2016;2:1441–9.
14. Sharp A, Coleman I, Yuan W, Sprenger C, Dolling D, Rodrigues DN, et al. Androgen receptor splice variant-7 expression emerges with castration resistance in prostate cancer. J Clin Invest 2019;129:192–208.
15. Guo Z, Yang X, Sun F, Jiang R, Linn DE, Chen H, et al. A novel androgen receptor splice variant is up-regulated during prostate cancer progression and promotes androgen depletion-resistant growth. Cancer Res 2009;69:2305–13.
16. Hu R, Dunn TA, Wei S, Isharwal S, Veltri RW, Humphreys E, et al. Ligand-independent androgen receptor variants derived from splicing of cryptic exons signify hormone-refractory prostate cancer. Cancer Res 2009;69:16–22.
17. Li Y, Chan SC, Brand LJ, Hwang TH, Silverstein KA, Dehm SM. Androgen receptor splice variants mediate enzalutamide resistance in castration-resistant prostate cancer cell lines. Cancer Res 2013;73:483–9.
18. Todenhofer T, Azad A, Stewart C, Gao J, Eigl BJ, Gleave ME, et al. AR-V7 transcripts in whole blood RNA of patients with metastatic castration resistant prostate cancer correlate with response to abiraterone acetate. J Urol 2017;197:135–42.
19. Armstrong AJ, Halabi S, Luo J, Nanus DM, Scher HI, Antonarakis ES, et al. Reply to Dirix L., De Laere B. et al, and Sharp A. et al. J Clin Oncol 2019;37:2184–6.
20. De Laere B, Ost P, Gronberg H, Lindberg J. Has the PROPHECY of AR-V7 been fulfilled? J Clin Oncol 2019;37:2181–2.
21. Dirix L. Predictive significance of androgen receptor splice variant 7 in patients with metastatic castration-resistant prostate cancer: the PROPHECY study. J Clin Oncol 2019;37:2180–1.
22. Sharp A, Porta N, Lambros MBK, Welti JC, Paschalis A, Raj GV, et al. Dissecting prognostic from predictive utility: circulating AR-V7 biomarker testing for advanced prostate cancer. J Clin Oncol 2019;37:2182–4.
23. Montgomery RB, Plymate SR. AR-V7 protein in circulating tumor cells: the decider for therapy? JAMA Oncol 2016;2:1450–1.
24. Plymate SR, Sharp A, de Bono JS. Nuclear circulating tumor cell androgen receptor variant 7 in castration-resistant prostate cancer: the devil is in the detail. JAMA Oncol 2018;4:1187–8.
25. Fizazi K, Tran N, Fein L, Matsubara N, Rodriguez-Antolin A, Alekseev BY, et al. Abiraterone acetate plus prednisone in patients with newly diagnosed high-risk metastatic castration-sensitive prostate cancer (LATITUDE): final overall survival analysis of a randomised, double-blind, phase 3 trial. Lancet Oncol 2019;20:686–700.
26. Hoyle AP, Ali A, James ND, Cook A, Parker CC, de Bono JS, et al. Abiraterone in "high-" and "low-risk" metastatic hormone-sensitive prostate cancer. Eur Urol 2019;76:719–28.
27. James ND, de Bono JS, Spears MR, Clarke NW, Mason MD, Dearnaley DP, et al. Abiraterone for prostate cancer not previously treated with hormone therapy. N Engl J Med 2017;377:338–51.
28. Armstrong AJ, Szmulewitz RZ, Petrylak DP, Holzbeierlein J, Villers A, Azad A, et al. ARCHES: a randomized, phase III study of androgen deprivation therapy with enzalutamide or placebo in men with metastatic hormone-sensitive prostate cancer. J Clin Oncol 2019;37:2974–86.
29. Davis ID, Martin AJ, Stockler MR, Begbie S, Chi KN, Chowdhury S, et al. Enzalutamide with standard first-line therapy in metastatic prostate cancer. N Engl J Med 2019;381:121–31.
30. Chi KN, Agarwal N, Bjartell A, Chung BH, Pereira de Santana Gomes AJ, Given R, et al. Apalutamide for metastatic, castration-sensitive prostate cancer. N Engl J Med 2019;381:13–24.
31. Chen X, Bernemann C, Tolkach Y, Heller M, Nientiedt C, Falkenstein M, et al. Overexpression of nuclear AR-V7 protein in primary prostate cancer is an independent negative prognostic marker in men with high-risk disease receiving adjuvant therapy. Urol Oncol 2018;36:161.
32. Li H, Wang Z, Xiao W, Yan L, Guan W, Hu Z, et al. Androgen-receptor splice variant-7-positive prostate cancer: a novel molecular subtype with markedly worse androgen-deprivation therapy outcomes in newly diagnosed patients. Mod Pathol 2018;31:198–208.
33. Qu Y, Dai B, Ye D, Kong Y, Chang K, Jia Z, et al. Constitutively active AR-V7 plays an essential role in the development and progression of castration-resistant prostate cancer. Sci Rep 2015;5:7654.
34. Kaczorowski A, Chen X, Herpel E, Merseburger AS, Kristiansen G, Bernemann C, et al. Antibody selection influences the detection of AR-V7 in primary prostate cancer. Cancer Treat Res Commun 2020;24:100186.
35. Li H, Zhang Y, Li D, Ma X, Xu K, Ding B, et al. Androgen receptor splice variant 7 predicts shorter response in patients with metastatic hormone-sensitive prostate cancer receiving androgen deprivation therapy. Eur Urol 2021;79:879–86.
36. Sowalsky AG, Sharp A, Trostel SY, de Bono JS, Plymate SR. AR-V7 biomarker testing for primary prostate cancer: the ongoing challenge of analytical validation and clinical qualification. Cancer Treat Res Commun 2021;28:100218.
37. Russo JW, Gao C, Bhasin SS, Voznesensky OS, Calagua C, Arai S, et al. Down-regulation of dipeptidyl peptidase 4 accelerates progression to castration-resistant prostate cancer. Cancer Res 2018;78:6354–62.
38. Welti J, Sharp A, Brooks N, Yuan W, McNair C, Chand SN, et al. Targeting the p300/CBP axis in lethal prostate cancer. Cancer Discov 2021;11:1118–37.
39. Welti J, Sharp A, Yuan W, Dolling D, Nava Rodrigues D, Figueiredo I, et al. Targeting bromodomain and extra-terminal (BET) family proteins in castration-resistant prostate cancer (CRPC). Clin Cancer Res 2018;24:3149–62.
40. Nguyen HM, Vessella RL, Morrissey C, Brown LG, Coleman IM, Higano CS, et al. LuCaP prostate cancer patient-derived xenografts reflect the molecular heterogeneity of advanced disease and serve as models for evaluating cancer therapeutics. Prostate 2017;77:654–71.
41. Welti J, Rodrigues DN, Sharp A, Sun S, Lorente D, Riisnaes R, et al. Analytical validation and clinical qualification of a new immunohistochemical assay for androgen receptor splice variant-7 protein expression in metastatic castration-resistant prostate cancer. Eur Urol 2016;70:599–608.
42. Cejas P, Xie Y, Font-Tello A, Lim K, Syamala S, Qiu X, et al. Subtype heterogeneity and epigenetic convergence in neuroendocrine prostate cancer. Nat Commun 2021;12:5775.
43. Detre S, Saclani Jotti G, Dowsett MA. "quickscore" method for immunohistochemical semiquantitation: validation for oestrogen receptor in breast carcinomas. J Clin Pathol 1995;48:876–8.
44. Kluin RJC, Kemper K, Kuilman T, de Ruiter JR, Iyer V, Forment JV, et al. XenofilteR: computational deconvolution of mouse and human reads in tumor xenograft sequence data. BMC Bioinf 2018;19:366.
45. Dobin A, Davis CA, Schlesinger F, Drenkow J, Zaleski C, Jha S, et al. STAR: ultrafast universal RNA-seq aligner. Bioinformatics 2013;29:15–21.
46. Bolger AM, Lohse M, Usadel B. Trimmomatic: a flexible trimmer for Illumina sequence data. Bioinformatics 2014;30:2114–20.
47. He MX, Cuoco MS, Crowdis J, Bosma-Moody A, Zhang Z, Bi K, et al. Transcriptional mediators of treatment resistance in lethal prostate cancer. Nat Med 2021;27:426–33.
48. Hanzelmann S, Castelo R, Guinney J. GSVA: gene set variation analysis for microarray and RNA-seq data. BMC Bioinf 2013;14:7.
49. Cancer Genome Atlas Research N. The molecular taxonomy of primary prostate cancer. Cell 2015;163:1011–25.
50. Consortium GT. The genotype-tissue expression (GTEx) project. Nat Genet 2013;45:580–5.
51. Quigley DA, Dang HX, Zhao SG, Lloyd P, Aggarwal R, Alumkal JJ, et al. Genomic hallmarks and structural variation in metastatic prostate cancer. Cell 2018;175:889.
52. Zhu Y, Sharp A, Anderson CM, Silberstein JL, Taylor M, Lu C, et al. Novel junction-specific and quantifiable in situ detection of AR-V7 and its clinical correlates in metastatic castration-resistant prostate cancer. Eur Urol 2018;73:727–35.
53. Karzai F, Walker SM, Wilkinson S, Madan RA, Shih JH, Merino MJ, et al. Sequential prostate magnetic resonance imaging in newly diagnosed high-risk prostate cancer treated with neoadjuvant enzalutamide is predictive of therapeutic response. Clin Cancer Res 2021;27:429–37.
54. Sharp A, Welti JC, Lambros MBK, Dolling D, Rodrigues DN, Pope L, et al. Clinical utility of circulating tumour cell androgen receptor splice variant-7 status in metastatic castration-resistant prostate cancer. Eur Urol 2019;76:676–85.
55. Bordeaux J, Welsh A, Agarwal S, Killiam E, Baquero M, Hanna J, et al. Antibody validation. BioTechniques 2010;48:197–209.
56. MacNeil T, Vathiotis IA, Martinez-Morilla S, Yaghoobi V, Zugazagoitia J, Liu Y, et al. Antibody validation for protein expression on tissue slides: a protocol for immunohistochemistry. BioTechniques 2020;69:460–8.
57. Sfanos KS, Yegnasubramanian S, Nelson WG, Lotan TL, Kulac I, Hicks JL, et al. If this is true, what does it imply? How end-user antibody validation facilitates insights into biology and disease. Asian J Urol 2019;6:10–25.
58. Leong AS, Leong TY. Standardization in immunohistology. Methods Mol Biol 2011;724:37–68.
59. Sowalsky AG, Xia Z, Wang L, Zhao H, Chen S, Bubley GJ, et al. Whole transcriptome sequencing reveals extensive unspliced mRNA in metastatic castration-resistant prostate cancer. Molecular Cancer Research: MCR 2015;13:98–106.

60. Hussain M, Mateo J, Fizazi K, Saad F, Shore N, Sandhu S, et al. Survival with olaparib in metastatic castration-resistant prostate cancer. N Engl J Med 2020; 383:2345–57.
61. Sweeney C, Bracarda S, Sternberg CN, Chi KN, Olmos D, Sandhu S, et al. Ipatasertib plus abiraterone and prednisolone in metastatic castration-resistant prostate cancer (IPATential150): a multicentre, randomised, double-blind, phase 3 trial. Lancet 2021;398:131–42.
62. Sowalsky AG, Ye H, Bhasin M, Van Allen EM, Loda M, Lis RT, et al. Neoadjuvant-intensive androgen deprivation therapy selects for prostate tumor foci with diverse subclonal oncogenic alterations. Cancer Res 2018;78:4716–30.
63. Montgomery B, Tretiakova MS, Joshua AM, Gleave ME, Fleshner N, Bubley GJ, et al. Neoadjuvant enzalutamide prior to prostatectomy. Clin Cancer Res 2017; 23:2169–76.
64. Li Y, Yang R, Henzler CM, Ho Y, Passow C, Auch B, et al. Diverse AR gene rearrangements mediate resistance to androgen receptor inhibitors in metastatic prostate cancer. Clin Cancer Res 2020;26:1965–76.
65. Viswanathan SR, Ha G, Hoff AM, Wala JA, Carrot-Zhang J, Whelan CW, et al. Structural alterations driving castration-resistant prostate cancer revealed by linked-read genome sequencing. Cell 2018; 174:433–47.